Politechnika Warszawska

Wydział Fizyki

Praca inżynierska

Badanie charakterystyk krzemowych detektorów paskowych w pomiarach rozpraszania elastycznego protonów w eksperymencie STAR

Characterization of silicon strip detectors used in measurement of elastic proton scattering in the STAR experiment at RHIC

Autor:

Magdalena Dobrowolska
nr albumu: 246 652

Opiekunowie naukowi:

dr Włodzimierz Guryn
dr inż. Daniel Kikoła

WARSZAWA 2016

fizyka techniczna

Warsaw University of Technology

Faculty of Physics

Bachelor of Science in Engineering

Diploma Thesis

Characterization of silicon strip detectors used in measurement of elastic proton scattering in the STAR experiment at RHIC

Badanie charakterystyk krzemowych detektorów paskowych w pomiarach rozpraszania elastycznego protonów w eksperymencie STAR

Author:

Magdalena Dobrowolska

nr albumu: 246 652

Supervisors:

dr Włodzimierz Guryn

dr inż. Daniel Kikoła

WARSAW 2016

PHYSICS.WUT

Oświadczenie o samodzielności wykonania pracy

Politechnika Warszawska
Wydział Fizyki

Ja, niżej podpisana:

Magdalena Dobrowolska, nr albumu: 246 652

studentka Wydziału Fizyki Politechniki Warszawskiej, świadoma odpowiedzialności prawnej, oświadczam, że przedłożoną do obrony pracę dyplomową inżynierską pt.:

Badanie charakterystyk krzemowych detektorów paskowych w pomiarach rozpraszania elastycznego protonów w eksperymencie STAR

wykonałam samodzielnie pod kierunkiem:

dr Włodzimierza Guryna
dr inż Daniela Kikoły

Jednocześnie oświadczam, że:

- praca nie narusza praw autorskich w rozumieniu ustawy z dnia 4 lutego 1994 o prawie autorskim i prawach pokrewnych oraz dóbr osobistych chronionych prawem cywilnym,
- praca nie zawiera danych i informacji uzyskanych w sposób niezgodny z obowiązującymi przepisami,
- praca nie była wcześniej przedmiotem procedur związanych z uzyskaniem dyplomu lub tytułu zawodowego w wyższej uczelni,
- promotor pracy jest jej współtwórcą w rozumieniu ustawy z dnia 4 lutego 1994 o prawie autorskim i prawach pokrewnych.

Oświadczam także, że treść pracy zapisanej na przekazanym nośniku elektronicznym jest zgodna z treścią zawartą w wydrukowanej wersji niniejszej pracy dyplomowej.

Warszawa, dnia 22 lutego 2016 r.

Oświadczenie o udzieleniu Uczelni licencji do pracy

Politechnika Warszawska
Wydział Fizyki

Ja, niżej podpisana:

Magdalena Dobrowolska, nr albumu: 246 652

studentka Wydziału Fizyki Politechniki Warszawskiej, niniejszym oświadczam, że zachowując moje prawa autorskie udzielam Politechnice Warszawskiej nieograniczonej w czasie, nieodpłatnej licencji wyłącznej do korzystania z przedstawionej dokumentacji pracy dyplomowej pt.

Badanie charakterystyk krzemowych detektorów paskowych w pomiarach rozpraszania elastycznego protonów w eksperymencie STAR

w zakresie jej publicznego udostępniania i rozpowszechniania w wersji drukowanej i elektronicznej[1].

Warszawa, dnia 22 lutego 2016 r.

[1] Na podstawie Ustawy z dnia 27 lipca 2005 r. Prawo o szkolnictwie wyższym (Dz.U. 2005 nr 164 poz. 1365) Art. 239. oraz Ustawy z dnia 4 lutego 1994 r. o prawie autorskim i prawach pokrewnych (Dz.U. z 2000 r. Nr 80, poz. 904, z późn. zm.) Art. 15a. "Uczelni w rozumieniu przepisów o szkolnictwie wyższym przysługuje pierwszeństwo w opublikowaniu pracy dyplomowej studenta. Jeżeli uczelnia nie opublikowała pracy dyplomowej w ciągu 6 miesięcy od jej obrony, student, który ją przygotował, może ją opublikować, chyba że praca dyplomowa jest częścią utworu zbiorowego."

Abstract

The Relativistic Heavy Ion Collider at Brookhaven National Laboratory on Long Island in New York State is an accelerator where heavy ions, like gold nuclei for example, are accelerated to relativistic speeds to probe a state of matter called a Quark-Gluon Plasma (QGP). The Solenoidal Tracker at RHIC (STAR) is one of two still operating multipurpose detectors, which measure different types of particles produced in collisions at RHIC. For RHIC run 15, the STAR experiment was equipped with a system of forward silicon micro-strip detectors mounted in vessels called Roman Pots. The Physics Program with Roman Pots is dedicated to measuring physics processes with forward protons in polarized proton-proton collisions and proton-nucleus collisions at the center of mass energy up to 510 GeV. One of its goals is to search for the existence of a gluonic bound state in the Double Pomeron Exchange Process. The primary goal of the thesis was to investigate characteristics of the silicon micro-strip detectors, to study the level of pedestal and noise and to determine the number of noisy channels. To accomplish that, a large number of pedestal runs were analyzed. This thesis briefly discusses the physics of semiconductor detectors and the structure of the silicon micro-strip detectors. The analysis of the cluster energies has been conducted to find the most favorable cuts and thresholds. The process of the background elimination is shown in this thesis. The study showed that the system works exceptionally well because the level of noise is very low and stable over time. Moreover, the observed variations of the noise are minimal and there are only two potentially hot channels out of about 20 000.

Keywords:

RHIC, Brookhaven National Laboratory, STAR, the silicon micro-strip detectors, The Physics Program with Roman Pots at STAR, noise, pedestal, cluster, elastic scattering of protons, semi-elastic scattering of protons, Pomeron, Double Pomeron Exchange Process

Streszczenie

Relatywistyczny Zderzacz Ciężkich Jonów (tzw. RHIC) w Brookhaven National Laboratory na wyspie Long Island w stanie Nowy Jork jest akceleratorem, w którym ciężkie jony (np. jony złota) są zderzane przy relatywistycznych prędkościach w celu badania stanu materii zwanego plazmą kwarkowo-gluonową (ang. Quark-Gluon Plasma). Detektor STAR (ang. Solenoidal Tracker at RHIC) jest jednym z dwóch obecnie działających detektorów, który ma za zadanie wykrywanie różnych typów cząsteczek wyprodukowanych w zderzeniach w akceleratorze RHIC. Podczas zbierania danych przez akcelerator RHIC w 2015 roku eksperyment STAR został wyposażony w system paskowych detektorów krzemowych zamontowanych w pojemnikach zwanych Roman Pots. Korzystając z tych urządzeń prowadzone są pomiary, mające na celu zbadanie procesów fizycznych zachodzących przy zderzeniach spolaryzowanych protonów i zderzeniach typu proton-jądro przy energii środka masy sięgającej 510 GeV. Jednym z celów tego programu jest poszukiwanie cząstki będącej stanem związanym gluonów (tzw. kuli gluonowej, ang. glueball), która może być produkowana w procesie podwójnej wymiany Pomeronu. Główną częścią tej pracy było opracowanie charakterystyki paskowych detektorów krzemowych, zbadanie poziomów tła i szumu oraz wyznaczenie najbardziej zaszumionych kanałów detektorów. W pracy została opisana fizyka półprzewodnikowych detektorów oraz budowa paskowych detektorów krzemowych. Analiza energii klastrów została przeprowadzona w celu określenia optymalnych progów i cięć, których zastosowanie jest niezbędne do usunięcia tła i szumów z danych fizycznych. W pracy przedstawiono proces eliminacji tła. Badania pokazały, że system działa bardzo dobrze, ponieważ poziom szumu jest niski, jego wartość jest stała w czasie, a obserwowane fluktuacje są niewielkie. Ponadto znaleziono tylko dwa potencjalnie zaszumione kanały spośród ponad 20 000.

Słowa kluczowe:

RHIC, Brookhaven National Laboratory, STAR, paskowe detektory krzemowe, szum, tło, klaster, elastyczne rozpraszanie protonów, quasi-elastyczne rozpraszanie protonów, Pomeron, Double Pomeron Exchange Process

Contents

List of figures

Acknowledgment

I would like to express my gratitude to my supervisors, Dr. Eng. Daniel Kikoła and Dr. Włodek Guryn, for their valuable advice, dedicated time and support in creating this thesis. I am also very grateful for their help in organizing my student internship in Brookhaven National Laboratory.

I also wish to thank the STAR experiment team for their support and friendly atmosphere during my stay in Brookhaven National Laboratory.

1. Introduction

1.1. RHIC

The Relativistic Heavy Ion Collider (RHIC [1]) at Brookhaven National Laboratory on Long Island in New York State is an accelerator which investigates processes occurring in the collisions of heavy ions (such as Au) up to a maximum center-of-mass energy of 200 GeV per nucleon and collisions of polarized protons at center-of-mass energy up to 510 GeV [2][3]. Particularly, RHIC is suitable to answer the interesting question about the origin of proton's spin. Originally, it was believed that the spin of a proton is the sum of the three constituent quarks' spins. The research determined, that only 25% of the proton's spin comes from quarks' spins. Experiments at RHIC demonstrated that other 40% of the proton's spin is carried by the gluons. The remaining fraction of the proton's spin still needs to be determined [2] [4]. More information about the spin program at RHIC can be found in [5].

RHIC has two independent rings (called Blue and Yellow) where particles are accelerated to the relativistic speeds. At six locations the rings intersect and the beams can collide [4]. Currently detectors are installed only in two interaction points: STAR [6] (at 6 o'clock) and PHENIX [7] (at 8 o'clock) [8]. The tasks of those experiments are to study properties of the nuclear matter in a wide range of energy, to study spin effects, elastic and semi-elastic collisions.

1.2. The STAR Experiment

The STAR detector (Solenoidal Tracker at RHIC), weighing 1200 tons, is a system of sub detectors created to detect and examine vast numbers of particles produced in collisions at RHIC to find signs of the Quark Gluon Plasma (QGP) and study its characteristics [9].

A system of forward silicon micro-strip detectors is a part of the STAR experiment [8]. The forward detectors are mounted in vessels called Roman Pots. The Physics Program with Roman Pots is dedicated to measuring spin dependence of elastic scattering of polarized protons as well as to searching for the existence of the gluonic bound state in the Double Pomeron Exchange Process [10].

2. Silicon Strip Detectors (SSD)

The detectors used in this experiment were designed and made by Hamamatsu Photonics except for one detector which was created at the BNL Instrumentation Division [11]. The operation of the micro-strip detectors of ionizing radiation is based on the p-n junction in reverse biased mode. A silicon micro-strip detector is built by putting parallel strips made of the p^+-type silicon on a bulk of the n-type silicon. The total thickness of the silicon bulk in detectors used in the Roman Pot Physics Program is 400 μm [11]. The backplane is made of the n^+-type of silicon. The width of the p^+-type strip is 70 μm [8]. The length of the silicon strip measuring y and x coordinate is 79.38 mm and 49.29 mm [12], respectively. The active area of the detector, S, is about 75 x 45 mm^2 [11]. The number of strips in x-view plane, measuring x coordinate, is 756 and plane which measures y coordinate (y-view plane) has 504 strips [12]. At the surface of the silicon micro-strip detector is a thin layer of the SiO_2 glass. Over the SiO_2 glass, the fan-in aluminum strips are placed [11]. The SiO_2 layer is a great insulator and all together with the aluminum strips and p^+-type silicon strips are a set of capacitors which allow detecting more events [8][12]. A particular property of the silicon micro-strip detectors is that they bias each strip by using polysilicon [11]. The cross section of the detector is shown in Figure 2-1.

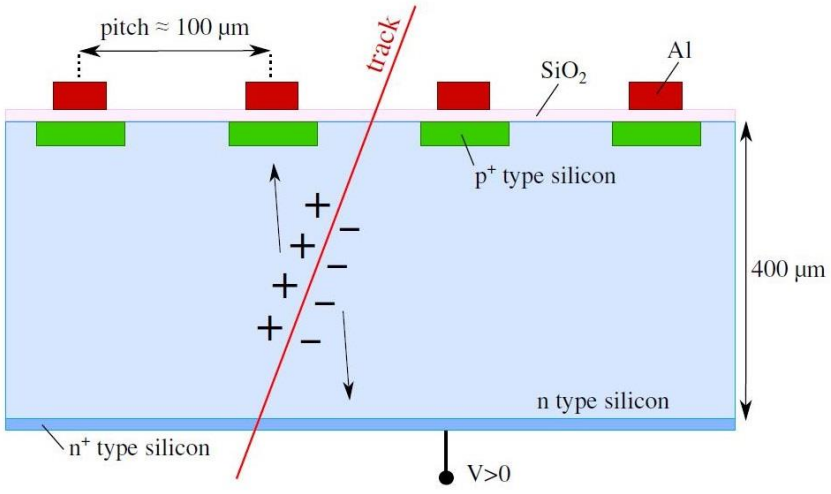

Figure 2-1: The cross-section of the SSD plane [3]

The red line depicts how a charged particle passes through the detector plane. The particle loses its energy through the ionization of atoms of the silicon. When a sufficient amount of energy is supplied, the electron-hole pairs are produced in the depletion region and electrons are excited to the conduction band leaving holes in the valence band. The depletion region is extremely important in the particle detection. If the electric field is big enough it prevents the recombination of electrons and holes so it takes carriers out of the depletion region: electrons flow to the n^+-type layer and holes drift to strips of the p^+-type of the silicon. Thanks to this, it is possible to find coordinates of the hit of the particle that passed through the detector. The p^+-type strips store the holes thus one needs to determine the strip number that has collected holes [12]. To determine accurately the two-dimensional position of the particle, two types of detectors are needed: measuring x and y coordinates. One Roman Pot houses 4 planes which have strips perpendicular with respect to each other so they are able to measure both x and y coordinates [12]. Figure 2-2 shows the trajectory of the particle passing through the detector planes. To increase the length of the depletion region, the p-n junction requires an external polarization. Without it, the depth of the depletion region has only a few microns and the capability of the detector is reduced. In Figure 2-1 one can observe that positive voltage is applied at the bottom of the n^+-type silicon layer, thus the p-n junction works in the reverse-biased mode. With the additional external voltage the depth of the depletion region can increase until the detector will be fully depleted. The voltage, for which the detector is fully depleted, is called a full depleted voltage and it is 100 V for the Physics Program with Roman Pots at STAR [12].

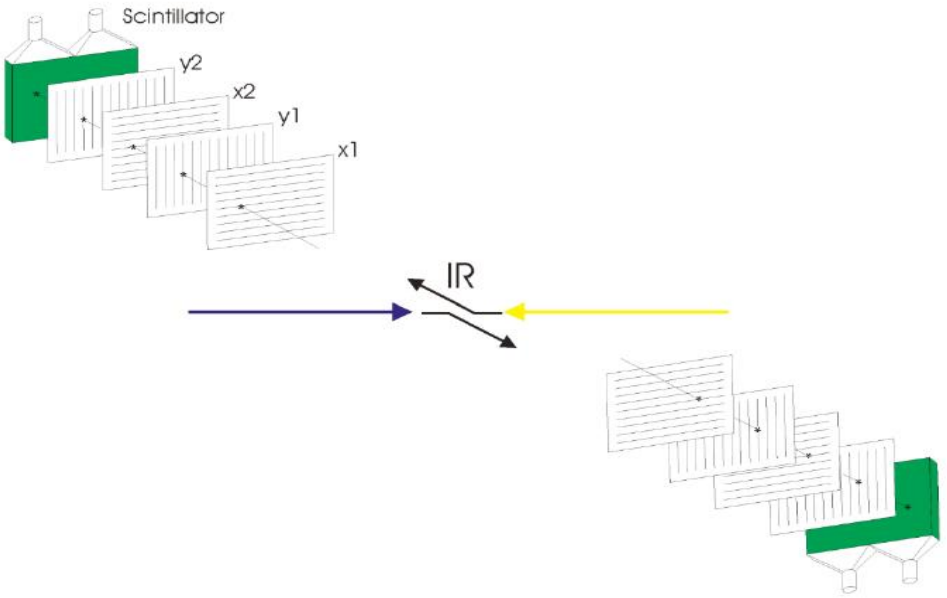

Figure 2-2: The trajectory of the particle passing though the detector planes [12]

The key parameter in the characterization of the SSDs is a strip pitch. The strip pitch is defined as a space between two adjacent strips. The value of the pitch affects the spatial precision so the smaller the gap the more precise the position of the particle. The pitch of the horizontal strips is 97.4 μm. The vertical strips have a pitch equal to 105 μm [3]. The width of the strips is also a significant feature that affects the resolution of the position measurement [8] [12].

The capacitance, C, is another important feature of the SSDs. In case of the Roman Pots, the capacitance is described by the formula for the parallel plate capacitors [12]:

$$C = \varepsilon \frac{S}{W} \tag{2.1}$$

where S is the detector's area, W is the junction width and ε is a permittivity. The capacitance is the main source of the noise level in the detector [12]. The charge fluctuations in the n-type bulk have also an impact on the noise level [2].

The silicon is the main material used to produce the micro-strip detectors due to a number of advantages of this material. The primary reason of using silicon

is that it is a semiconductor with the band gap of 1.12 eV. It is sufficiently large, that noise caused by a thermal generation of the charge carriers is very low, allowing the use of detectors at the room temperature without cooling. The SSDs are commonly used in the particle physics because the energy needed to create the electron-hole pairs is 3.62 eV [12] and this value is small in comparison with other detectors. The essential feature of the silicon is its comparatively high density. Thanks to this property, sensors can detect the precise two-dimensional position of the particle [8]. Significant advantages of the silicon are also its good mechanical properties.

The main disadvantage of this type of detector is that they become damaged due to the radiation. The silicon is also popular because of the low price and because it is widespread [13].

3. The Physics Program with Roman Pots

3.1. Introduction

As mentioned in the section 1.2, the STAR detector uses a set of Roman Pots to collect data on the elastic or quasi-elastic collisions of polarized protons. The polarization of the beam at RHIC is up to 70%, which gives a unique opportunity to examine processes where protons stay intact after the collision. The structure of the Roman Pots permits to register the smallest possible scattering angles, θ, hence a squared four-momentum transfer between incoming and outgoing protons, t, can be extended to the small and medium values. Moreover, the usage of the beam of highly polarized proton helps to investigate the unexplored spin dependence of the diffraction. The processes of interest in the proton-proton interactions in the Physics Program with Roman Pots are, for example, the elastic scattering (the elastic collision) and the Central Production (the quasi-elastic collisions) [10].

The interaction between hadrons can be divided into two groups: the hard and soft processes. The hard processes take place when the four momentum transfer [3],

$$t = (p_1' - p_1)^2 \tag{3.1}$$

is sufficiently large, of the order of a few GeV/ c^2 and higher. The soft processes appear when |t| is lower. Here, p_1 is the value of the momentum before the scattering and p_1' is the value of momentum after the scattering.

3.2. Elastic scattering of the polarized protons

For the process with two bodies, the reaction can be written as [3]:

$$A + B \rightarrow A' + B' \tag{3.2}$$

It is seen that after the elastic scattering is no new products and particles stay intact after the collision.

The diagram of the elastic proton-proton scattering presented in Figure 3-1 shows that the elastic scattering of protons occurs via an exchange of the colorless

objects with the quantum numbers of the vacuum, historically called a Pomeron. In perturbative QCD, the Pomeron is a theoretical object which describes the exchange of the gluons [14]. The Physics Program with Roman Pots at STAR is dedicated to study the proton-proton elastic scattering in center-of-mass energy, $\sqrt{s}$ ranging from 50 GeV to 510 GeV [2] and t in range from the Coulomb Nuclear Interference region, $4 \cdot 10^{-4} < |t| < 0.12\ (\mathrm{GeV})^2$ [12] to 1.5 $(\mathrm{GeV})^2$ [10]. An exploration of the spin dependence of the proton-proton scattering with a small momentum transfer and RHIC energies gives a chance to obtain information about the Pomeron [10].

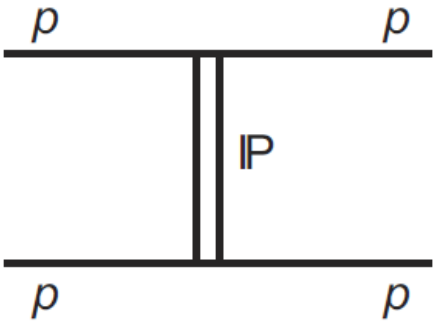

Figure 3-1: The elastic scattering of protons [14]

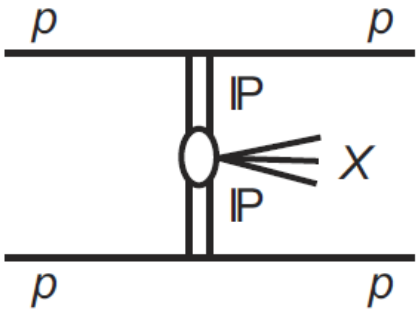

Figure 3-2: The Central Production [14]

A scattering amplitude A(s,t) carries information about a differential cross section, $\frac{d\sigma}{dt}$, and it depends on a squared center of mass energy s and t. The differential cross section is defined as:

$$\frac{d\sigma}{dt} = \frac{1}{16\pi s^2}|A(s,t)|^2 \tag{3.3}$$

s is written as:

$$s = (p_1 + p_2)^2 \tag{3.4}$$

where p_1, p_2 are four-momenta before the elastic interaction and p_1', p_2' are four-momenta after the elastic interaction.

The four-momentum transfer after the transformation takes the form:

$$t = (p_1' - p_1)^2 = -4p^2 \sin^2 \frac{\theta}{2} \tag{3.5}$$

where p is the absolute value of the momentum. For the low scattering angles:

$$\sin \frac{\theta}{2} \overset{\theta \to 0}{\longrightarrow} \frac{\theta}{2} \tag{3.6}$$

and t limits to [3]:

$$t \approx -p^2\theta^2 \tag{3.7}$$

3.3. Central Production

The second process of interest in the Physics Program with Roman Pots is the Central Production. The Central Production Process, depicted in Figure 3-2, occurs during the Double Pomeron Exchange Process (DPE). Each proton emits one Pomeron and each Pomeron carries a fraction of proton momentum ξ. Emitted Pomerons interact with each other resulting in production of a massive recoil system M_x. The reaction of this phenomenon is given as [10]:

$$p + p \rightarrow p + M_x + p \tag{3.8}$$

Under the certain conditions, this massive system forms as a glueball or states coupling with gluons which could be produced with depleted background as against to standard hadronic production processes. The primary aim of investigation of the Central Production Process is to search and study the particles produced in the Double Pomeron Exchange Process [10]. The glueball is a hypothetical particle, whose existence is foreseen by QCD. It consists only of the gluons without the valence quarks. In terms of QCD, glueballs have a neutral color charge by analogy to mesons and baryons since they are composed of two or three gluons [15].

3.4. The layout of forward detectors

The Roman Pots (RPs) are the cylindrical vessels and each Roman Pot houses a Silicon Strip Detector package (SSD) consisting of 4 silicon planes (two x-view detectors with vertical strips and two y-view detectors with horizontal strips) and a trigger counter. To read data from each plane the system uses 160 SVXIIE readout chips (abbreviated to SVX in this thesis). Each SVX chip has 128 input channels and 126 or 128 strips connected to it. The Hamamatsu detectors are designed to have 126 strips connected to one readout SVX chip, channels 2-127, because the edge channels in the SVX chip have more noise than other channels [2], so the end channels of the chip could be left unbounded [11]. Also, one plane E2DA (SVX chips number 60-63) which was installed on January 2015, has an old BNL detector on it and in this version all 128 SVX chip channels are connected to the silicon and included in the analysis [11]. A silicon plane, SVXIIE chips and drivers or receivers are glued on a detector board. The detector boards are shown in Figure 3-3. The trigger counter is a scintillator connected to two photomultiplier tubes. The whole detecting system consists of 8 RPs placed far enough from the interaction point (IP) where scattered protons are well separated from the beam so they can be detected. During data taking period with the Roman Pots in 2015 vessels were positioned vertically on both sides of the STAR detector at 15.8 and 17.6 m from the interaction point. The layout of the system is shown in Figure 3-4. Labels E1U, W1U etc. are the names of the Roman Pots, which will be described in detail in section 3.6.

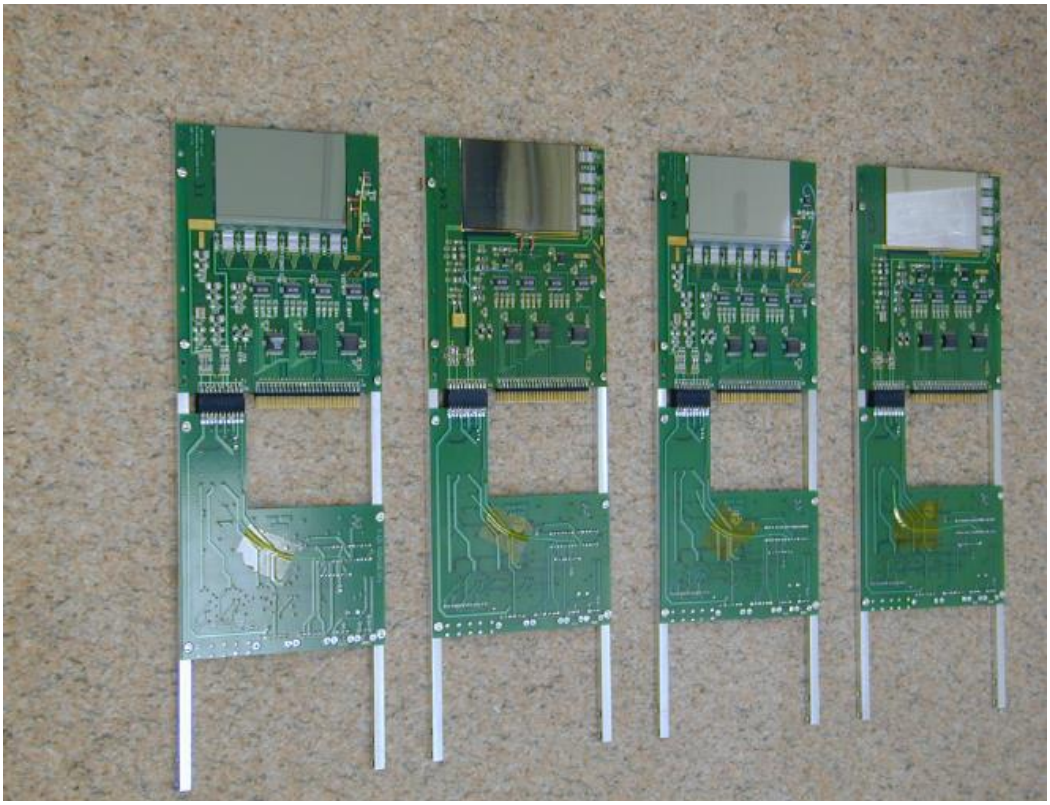

Figure 3-3: Detector boards [8]

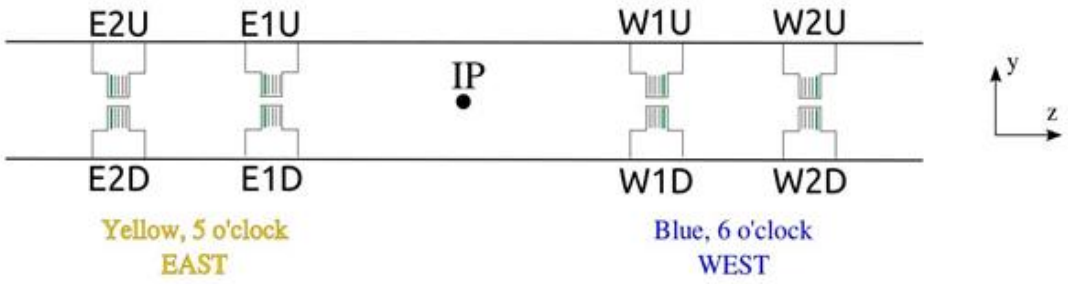

Figure 3-4: The layout of the Roman Pots detectors in the STAR experiment [16]

3.5. Roman Pots

The main advantage of the Roman Pots is that the Silicon Strip Detector package can be set close to the beam without a loss of the vacuum in the beam pipe while the interior of the vessel is under the atmospheric pressure. The greater the energy of polarized protons, the smaller the scattering angles of protons.

Consequently, one needs to employ the detector which can be moved closer or further from the beam of protons [8]. In Figure 3-5 the Roman Pots are presented and each one consists of: a pot, a window frame and a 300 μm thin stainless steel window. The task of the frame is to prevent the window from deforming when the vessel is put in the beam pipe. The thickness of the window is small to minimize the material which protons have to pass through [12].

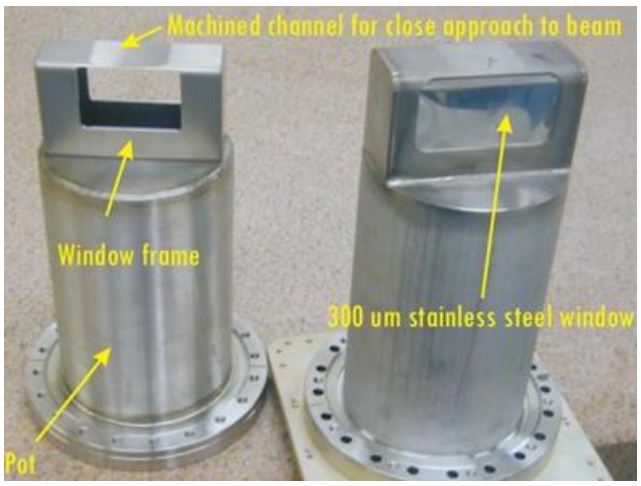

Figure 3-5: The Roman Pots [8]

3.6. Naming convention of the Roman Pots and the Si planes

Three characters are assigned to name the Roman Pots. Eight vessels are positioned vertically on both sides of the STAR detector. The first letter of the label refers to the side where the package was located – east (E) in the yellow beam or west (W) in the blue beam. The second character, a digit, tells of the station position with respect to the interaction point - closer (1) or further (2). The last one denotes whether the RP was installed up (U) or down (D) with regard to the beam pipe.

The Silicon Strip Detector planes are named accordingly to the labels of the Roman Pots where they are mounted. To specify an individual plane the capital letter A, B, C or D (with respect to the interaction point) is added to the label of housing Roman Pot [16]. For example, the first plane of the W2D detector is called W2D-A. Figure 3-6 shows the system layout. The readout of the SVX II chips by associated Sequencers (SEQ) is also shown.

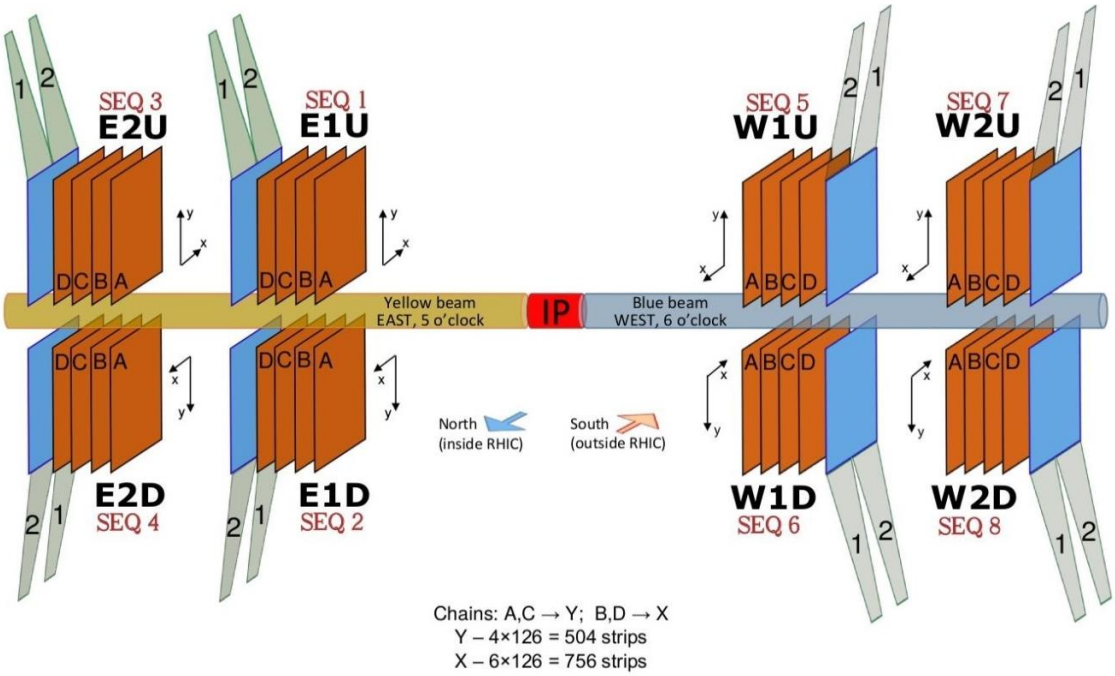

Figure 3-6: The layout of the detecting system [16]

4. Pedestal and noise level analysis

4.1. Introduction

To measure the signal of an ionizing particle, the noise has to be accounted for and subtracted from the signal registered by the Silicon Strip Detectors. The noise is generally described by two quantities: the pedestal value and random noise described as the standard deviation of pedestal value. The pedestal is the value of the signal that is always present in the detector. The pedestal and noise were determined from a special set of "pedestal" data runs. For each channel the pedestal P_{ij} of the i^{th} channel j^{th} SVX chip is calculated from:

$$P_{ij} = \frac{1}{N}\sum_{k=1}^{k=N} P_{ijk} \tag{4.1}$$

where N is the total number of events in the pedestal run and P_{ijk} is the signal of i^{th} channel j^{th} SVX chip of the k^{th} event.

Why information about the pedestal is so important? Firstly, the accurate pedestal value should be subtracted from the physics data obtained in the physics run. Secondly, the standard deviation of the mean of the pedestal value, denoted by σ (sigma), is a measure of the random (statistical) noise of the detector:

$$\sigma_{ij} = \sqrt{\frac{1}{N}\sum_{k=1}^{k=N}\left(P_{ijk} - P_{ij}\right)^2} \tag{4.2}$$

where σ_{ij} is sigma value of the i^{th} channel and j^{th} SVX chip. Both the pedestal and the statistical noise are necessary to account for the noise in the detector in the measurements.

There were 81 special runs held in the first half of 2015 dedicated to obtaining information about the pedestal values. This type of run is called a pedestal run. The pedestal run was taken when there was no beam in the accelerator hence no particles were going through the detectors. After each

pedestal run were a few physics runs which were using data from the corresponding pedestal run to subtract pedestal value channel by channel.

To determine the value of the signal for the physics analysis, a number of steps had to be undertaken. First, the ranges of the pedestal and random noise have to be determined. The second step was to check whether levels of the pedestal and noise are stable over time as well as if there are some irregularities from the average pedestal and noise values. The next important action was to analyze anomalies I found and identify problems they may cause them. The next step was to determine if there were channels with high noise levels in order to decide whether they should be excluded from analysis. The next step was to establish a few conditions to get rid of hits that come from noise.

Overall, the detectors and the SVX chips have been working exceptionally well. Only one out of 160 SVX chips (SVX chip number 043) was not working properly and it was disconnected and excluded from analysis.

4.2. Tools used for analysis

The study of each pedestal run was performed using information stored in the two-dimensional histograms of the pedestal values for each channel for all SVX chips. An example of such two-dimensional histogram for a given SVX chip is shown in Figure 4-1. The X axis represents the ADC value which is ADC value obtained from the analog to digital converter. The ADC (analog-to-digital) value is approximately proportional to the energy deposited in the detector. The Y axis represents the channel number of a given SVX chip. The software for the data analysis was written in C++ using the ROOT framework libraries [17]. The macro reads previously mentioned histograms files and generates a set of different histograms for each pedestal run. Pedestal and noise are analyzed in many aspects; for example: the histograms presenting an overview of the pedestal or sigma values, the files containing information about channels which are candidates to be noisy channels, pedestal and sigma values compared with average values obtained from the STAR Data Base. All those analyses are described in details in this thesis. I was also provided by the STAR team with a few macros using ROOT and root4star libraries which I modified and extended to perform my analysis.

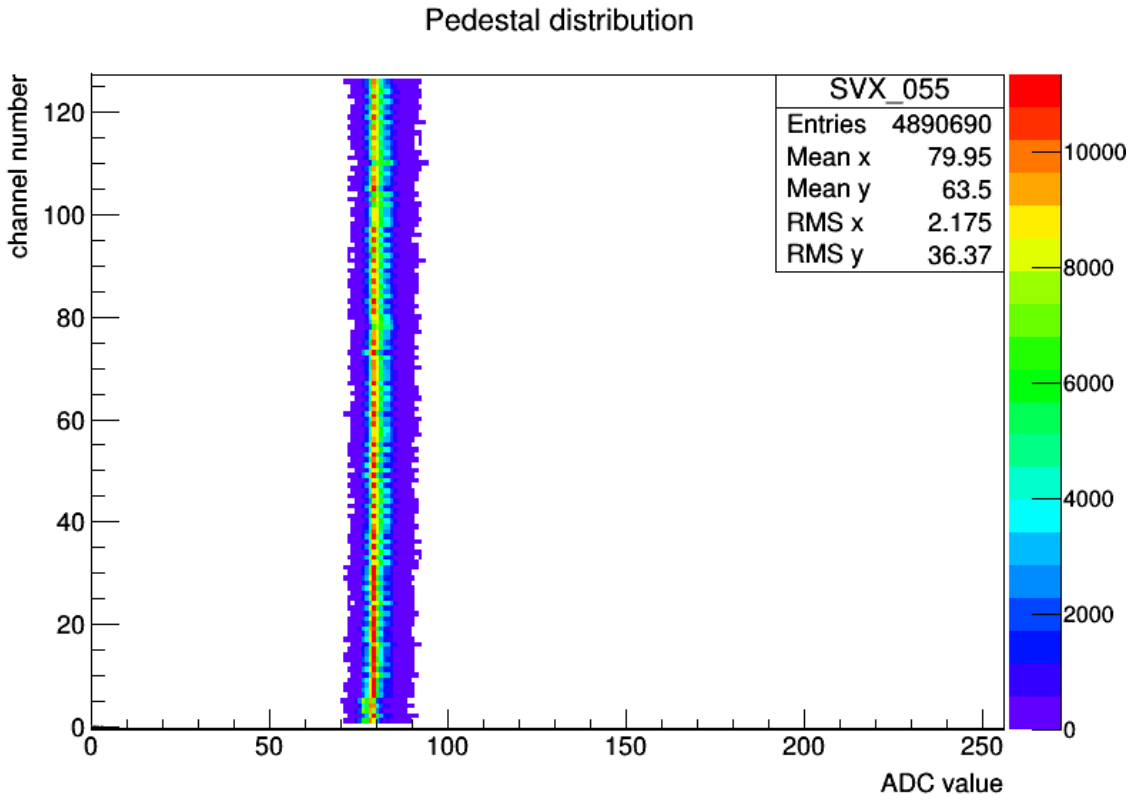

Figure 4-1: Two-dimensional histogram of the pedestal (represented as ADC value) for channels in the SVX chip number 55

4.3. Search for the possible anomalies

The histogram presented in Figure 4-1 is a representative of a typical pedestal distribution: it does not show any irregularity and the pedestal value for all strips has nearly a constant value. The vast majority of the SVX chips have pedestal distribution as shown in Figure 4-1 but not all the histograms looks like this one. Figures 4-2, 4-3, 4-4, 4-5 show some anomalies, which was observed. One can see in Figure 4-2 that for some channels pedestal has different values than for other channels. Another feature that was found was that for some SVX chips were low and high-ADC value readings. This issue is presented in Figure 4-3 for SVX chip number 046. Higher ADC values for some channels for a given SVX chip have also been classified as a certain irregularity. Figure 4-4 and 4-5 show distributions with higher pedestal values for a few of the first and last channels, respectively, but these anomalies are not a problem since the true pedestal values were subtracted for data analysis.

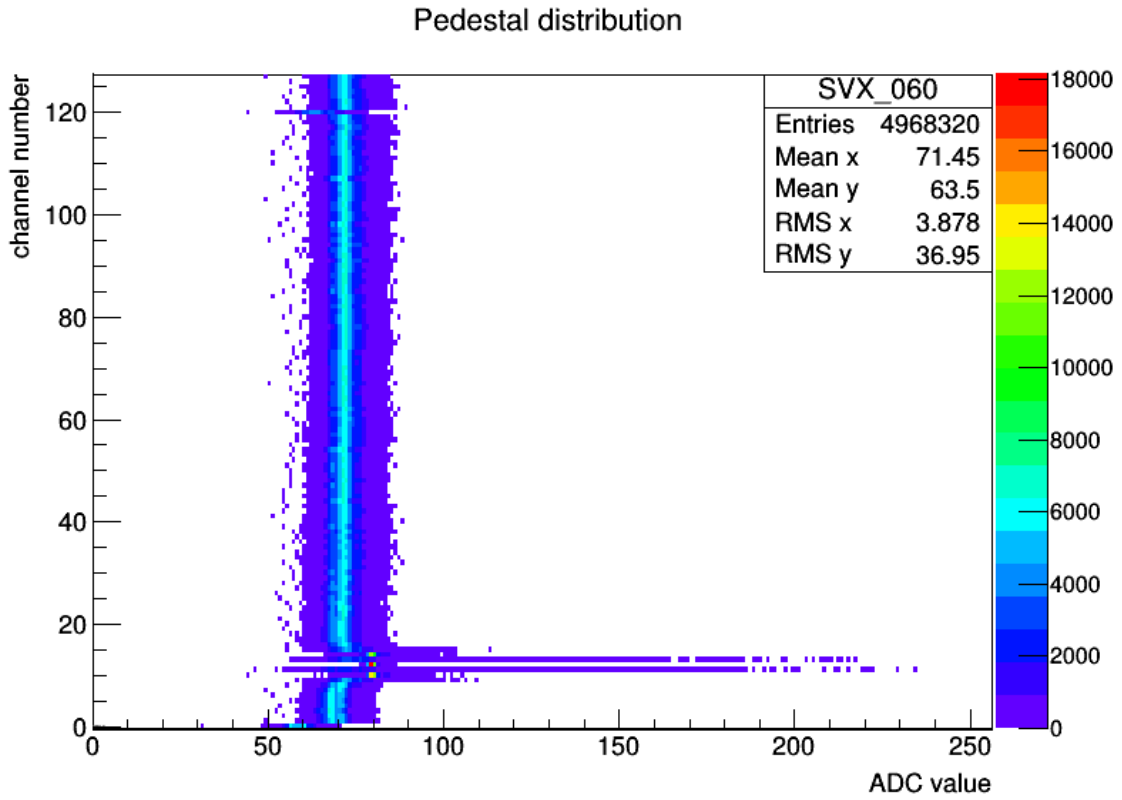

Figure 4-2: The pedestal distribution with different values of ADC for a few channels

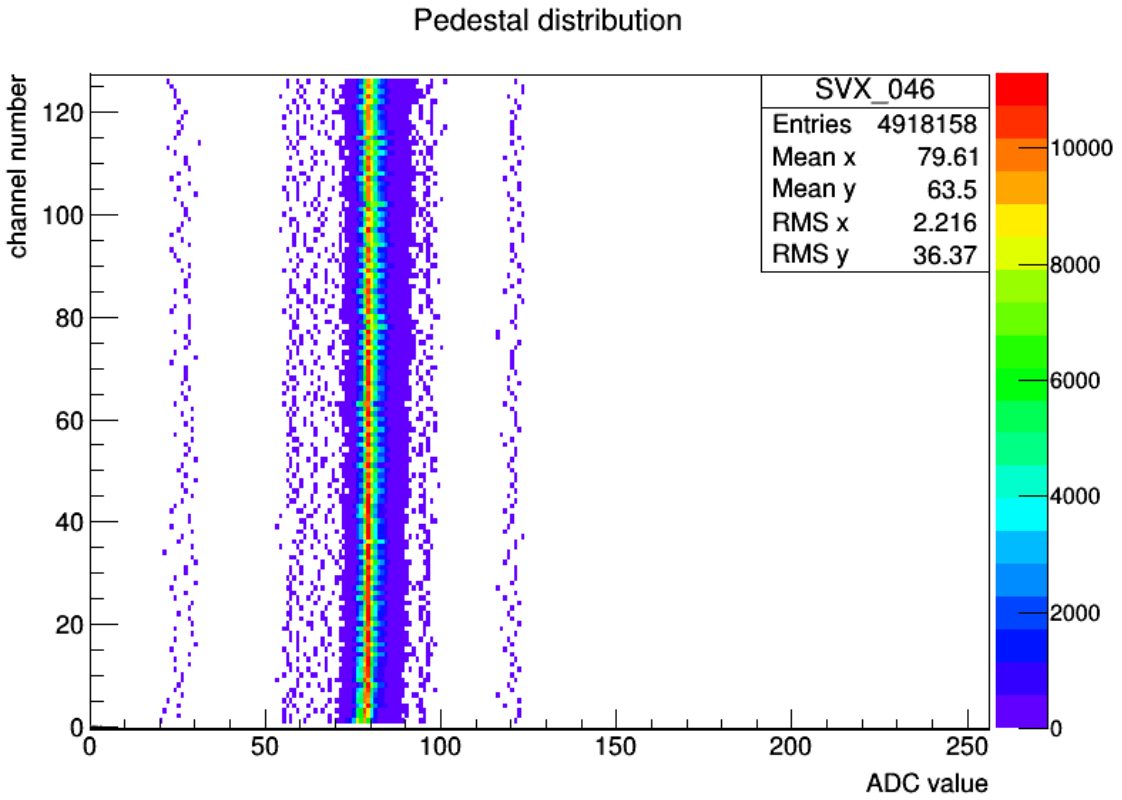

Figure 4-3: The pedestal distribution with the low and high-ADC value readings

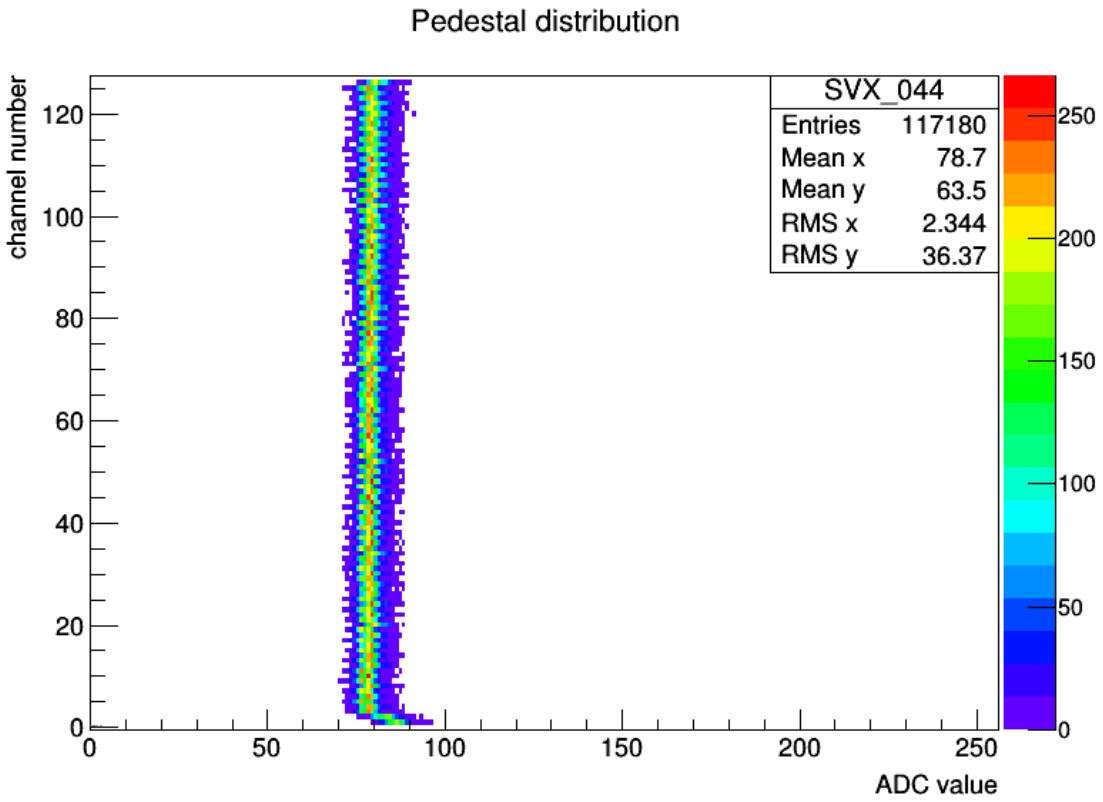

Figure 4-4: The pedestal distribution with higher ADC values for a few of the first channels

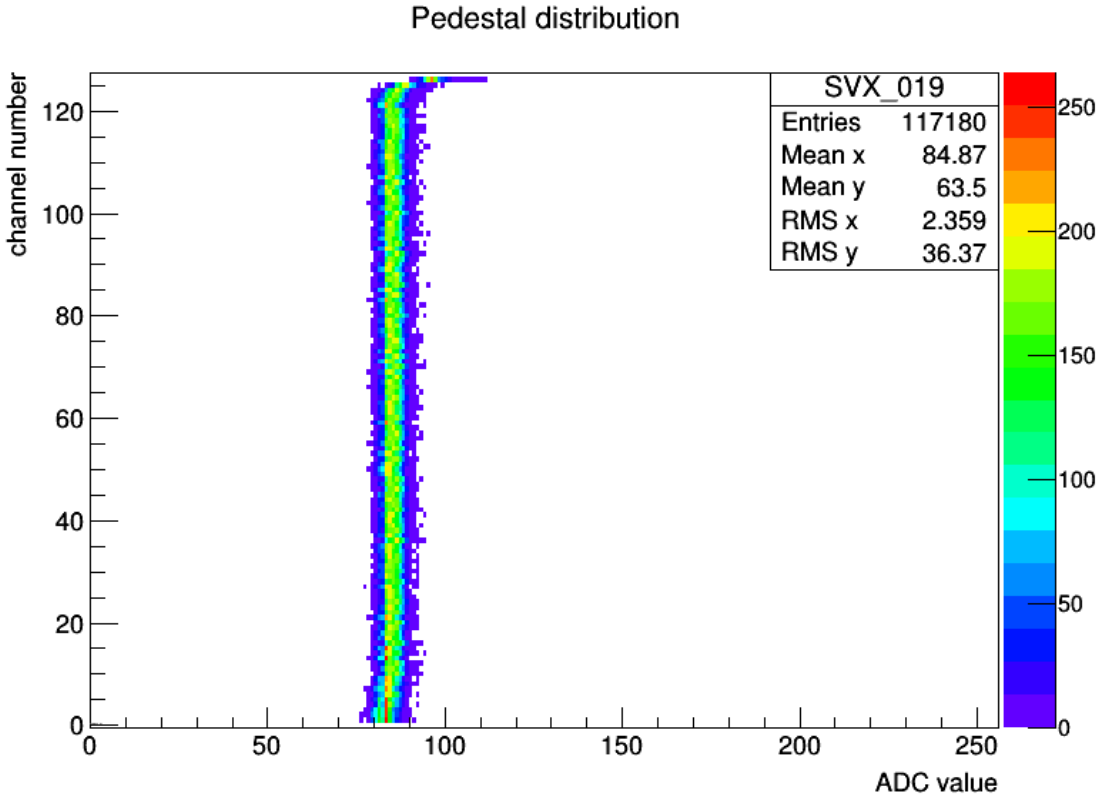

Figure 4-5: The pedestal distribution with higher ADC values for a few of the last channels

4.4. *Determination of the pedestal and noise level*

The thorough analysis was done for all (~20,000) channels. For each channel the pedestal (ADC value) distribution was analyzed. Figure 4-6 shows the example pedestal distribution for a given channel. The distribution is approximately Gaussian (with that function data are described well). The Gaussian fit is commonly used in the data analysis because the normal distribution describes the random cases and the pedestal distribution for a given channel can be considered to be random. Two parameters describe the Gaussian distribution: mean value of the distribution denoted by μ and standard deviation σ of the distribution. In terms of pedestal distribution the mean value is the average pedestal P_{ij} of the i^{th} channel and j^{th} SVX chip and σ_{ij} (sigma), is the random (statistical) noise of the detector.

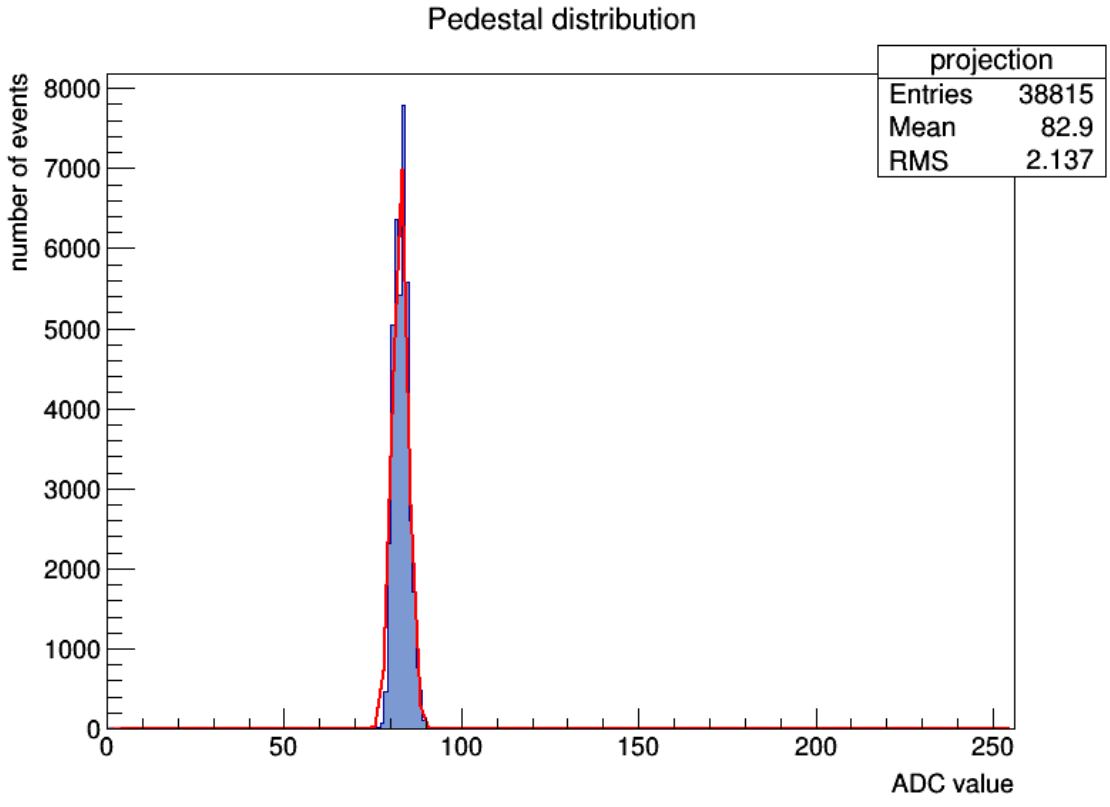

Figure 4-6: The distribution of the pedestal values for one channel

Figure 4-7 presents that average pedestal value (mean of the Gaussian fit) is relatively constant for a given plane. The further analysis showed that only for plane W1D-C strips connected to SVX chip number 113 have pedestal value lower than other strips on this plane. Again this is not a problem since the pedestals are subtracted on channel-by-channel basis. Moreover, they are basically constant for each SVX chip.

Another study was performed to check the fluctuation of the average pedestal level for all SVX chips. The average value of the pedestal was retrieved from the Gaussian fit. From Figure 4-8 one can observe that the pedestal for each channel for all SVX chips is in the range from about 70 to 90 ADC counts depending on Roman Pot. The study of 81 pedestal runs confirmed that from run to run the range of the pedestal value is similar and the pedestals are stable during all the data taking period.

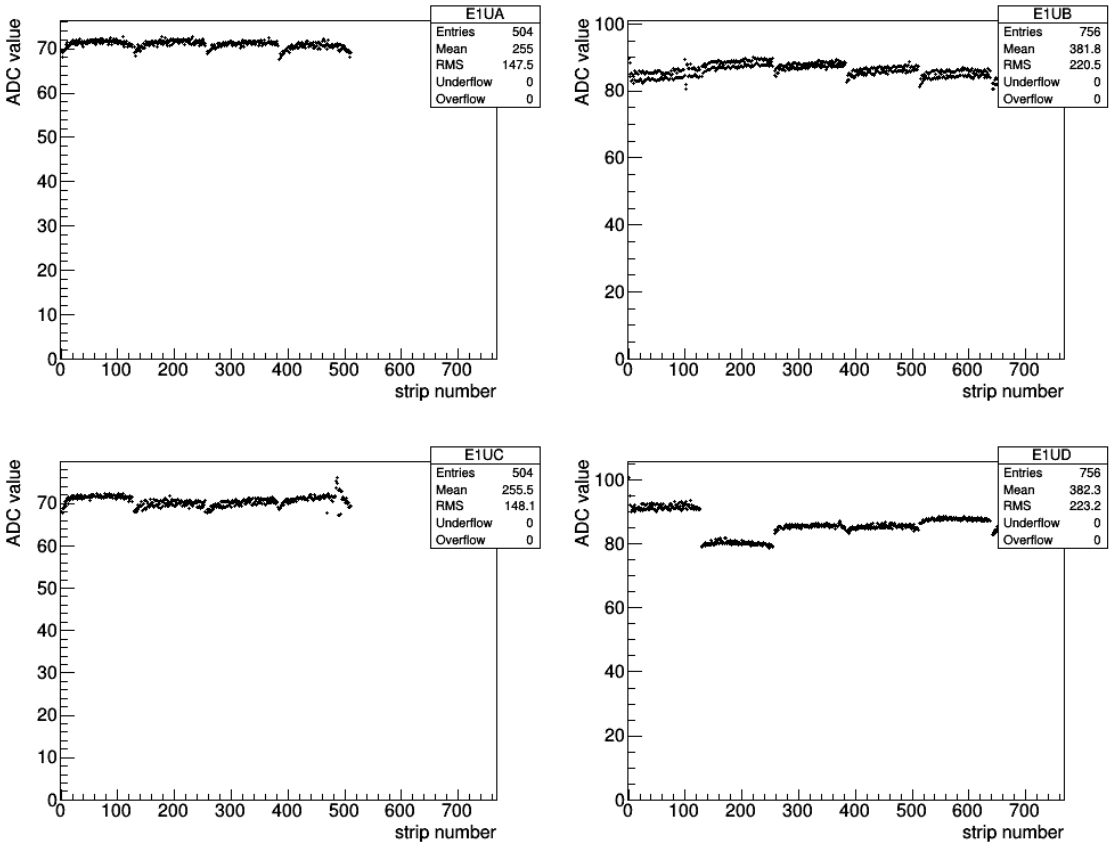

Figure 4-7: The average pedestal values for Roman Pot number E1U as a function of channel number

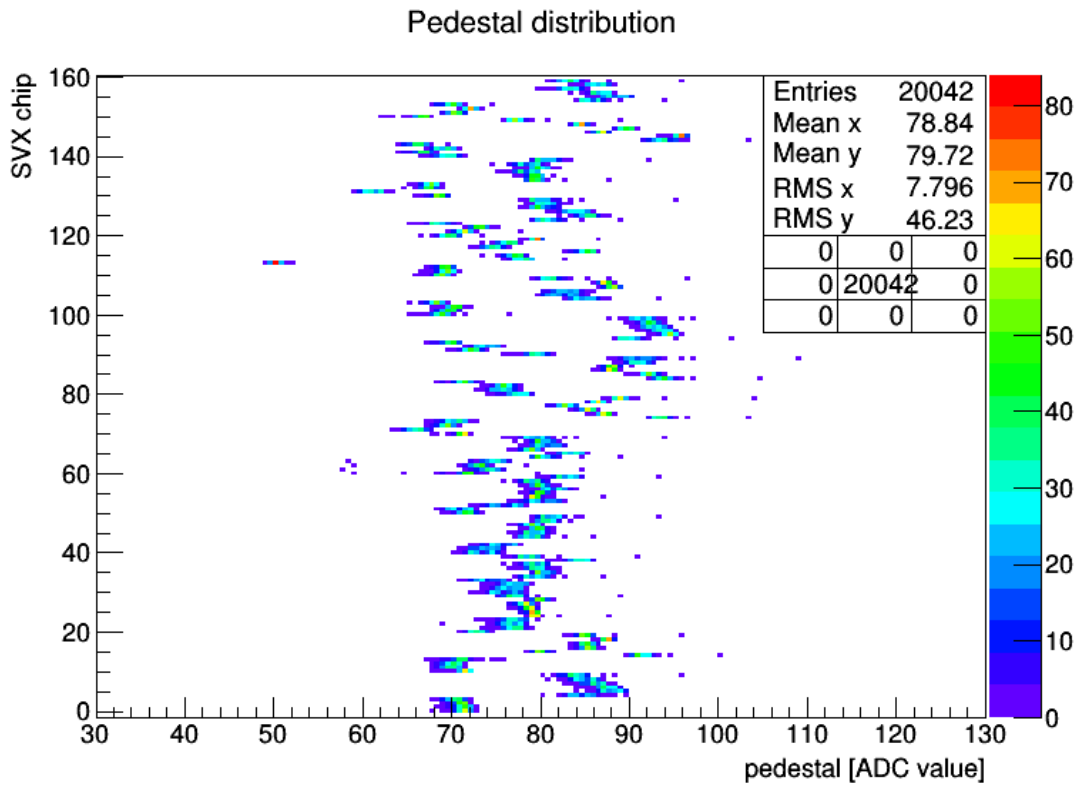

Figure 4-8: The distribution of pedestal for a single pedestal run

A study was done to determine the level of the random noise. The histogram showed in Figure 4-9 presents that the statistical noise level, as measured by the σ from the fit, is similar in one plane. Further studies did not show any irregularity; the σ value is stable over time for a given Roman Pot. The variations among the channels are a fraction of an ADC count. The histograms in Figure 4-10 and Figure 4-11 provide the information about the diversity of the σ (obtained from the Gaussian fit) values for all SVX chips for a given pedestal run. Based on Figure 4-9, Figure 4-10 and Figure 4-11 one can easily see the σ value fluctuates around 2 ADC counts. The mean of the distribution is 2 ADC counts and the RMS is about 0.3 ADC counts. In Figure 4-11 the log scale is on the y-axis.

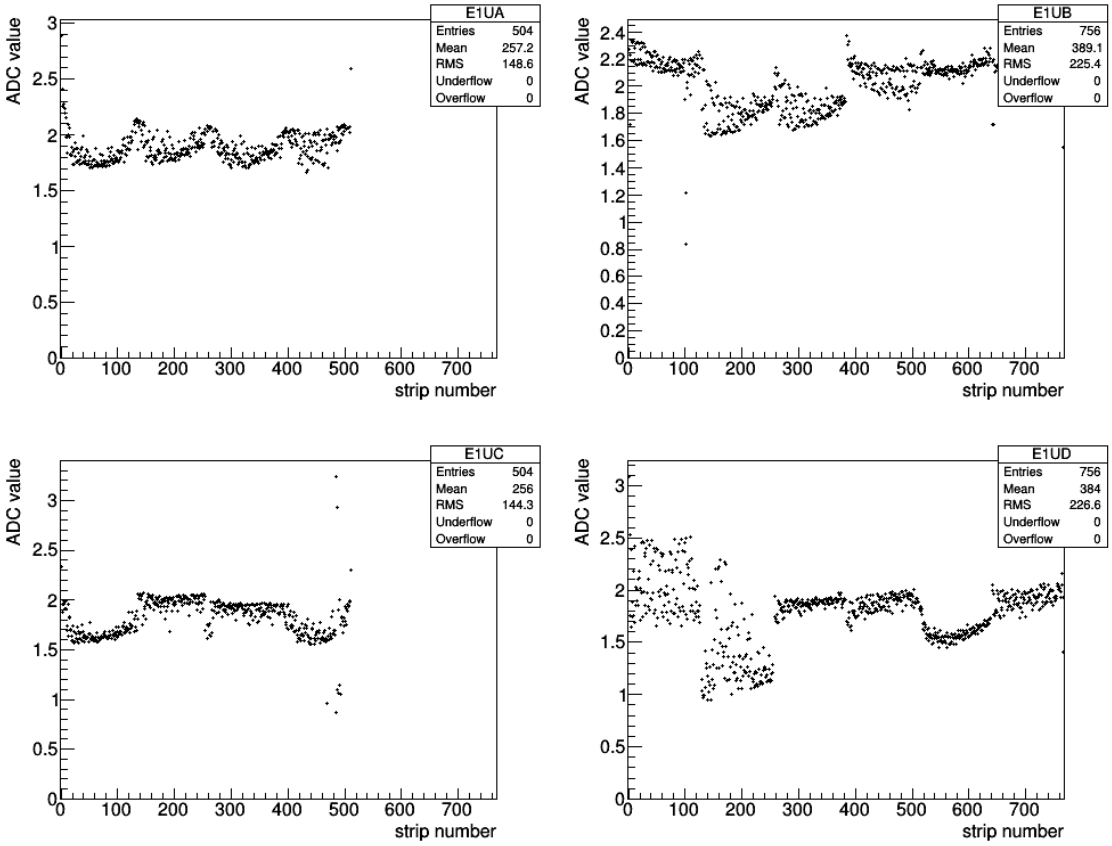

Figure 4-9: Sigma values for Roman Pot number E1U as a function of channel number

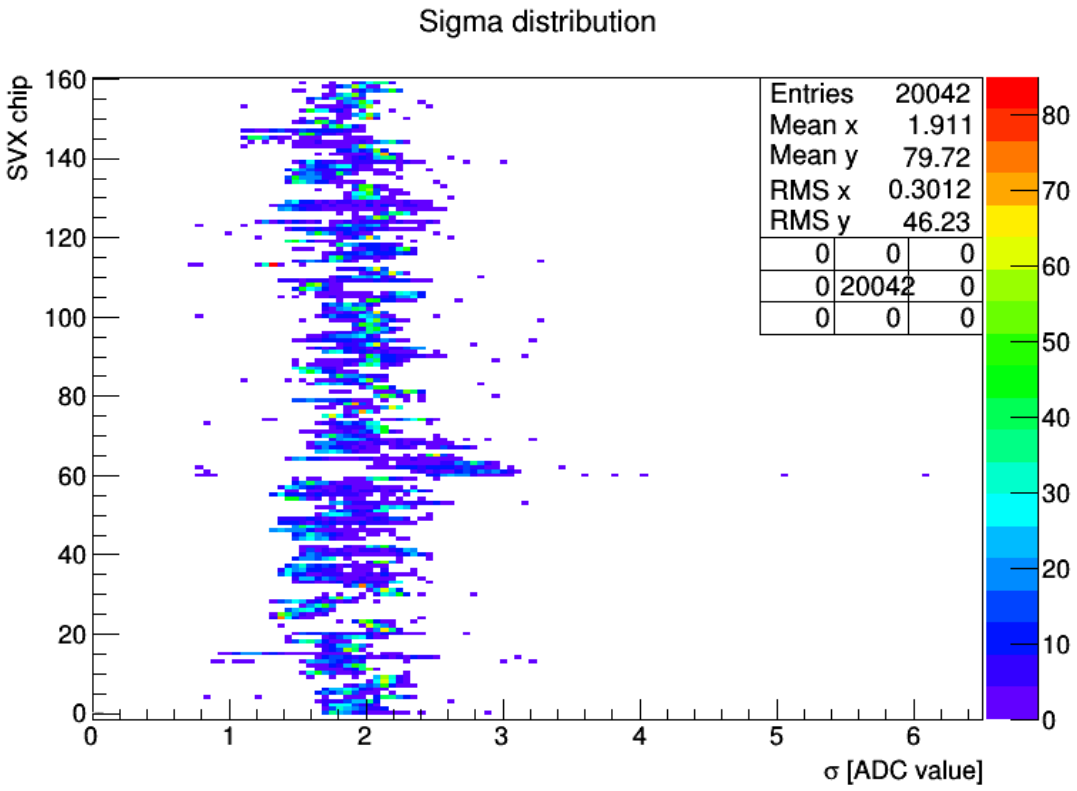

Figure 4-10: The distribution of sigma value for a single pedestal run

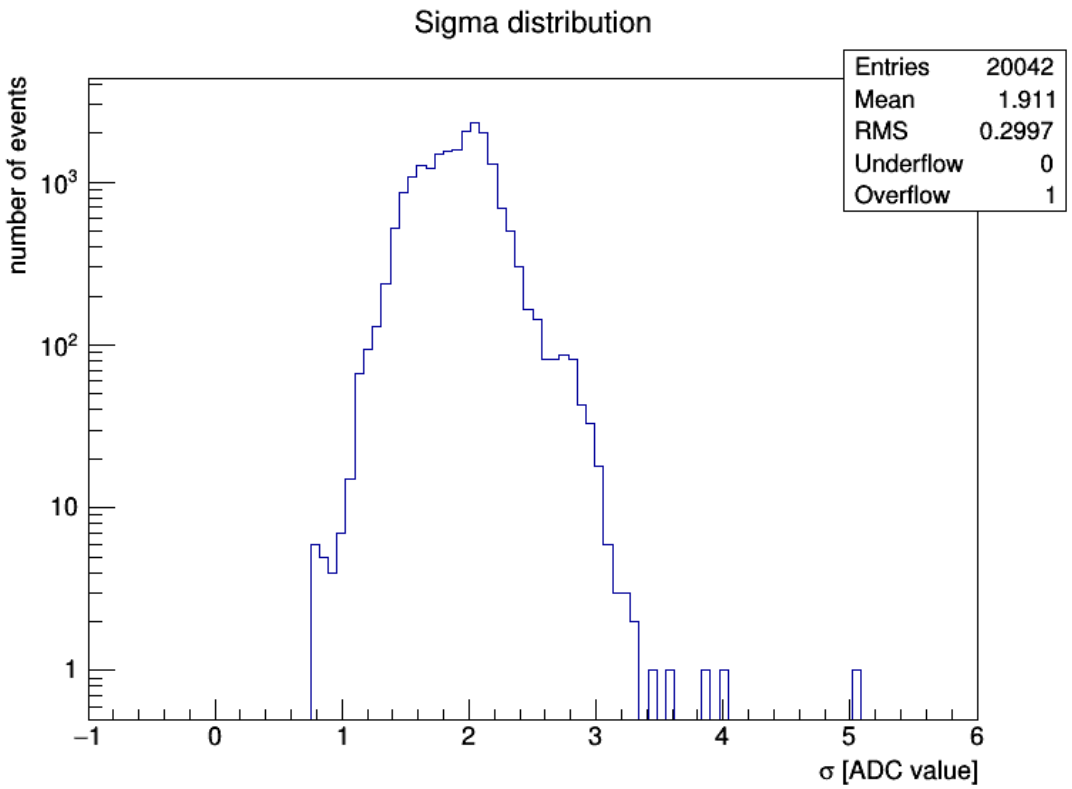

Figure 4-11: The distribution of sigma value for a single pedestal run

4.5. Evaluation of non-Gaussian features of the pedestal distribution

Another valuable part of the characteristic was to check how much the mean value of the Gaussian fit differs from the mean value of the histogram. The result of this study is presented in Figure 4-12, the mean of the presented histogram is around 0.17 ADC counts. Therefore the assumption that the Gaussian fit is valid for the pedestal distribution is correct for this case. The result was confirmed for all the pedestal runs. Only two out of 20 000 channels have a deviation more than 3 ADC counts as shown in Figure 4-12.

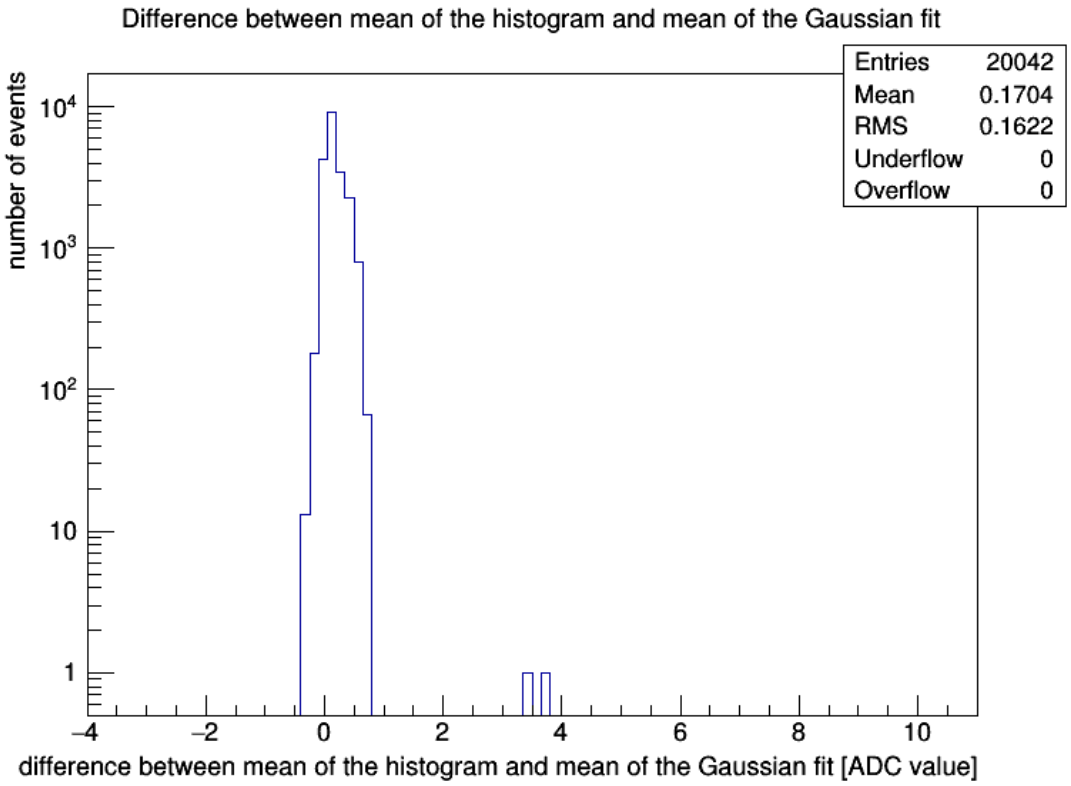

Figure 4-12: The difference between mean of the histogram and mean of the Gaussian fit

Another check was done by determining the skewness of the pedestal ADC distribution for each channel. The skewness gives information whether the distribution differs from Gaussian distribution. The histogram is skewed to the left (the negative skewness) when the left tail is longer than the right one, if the right tail is longer than the left tail then the distribution is skewed to the right (the positive skewness) [18]. Figure 4-13 shows the distribution of the skewness for one pedestal run. The analysis of 81 pedestal runs showed that the average value of the skewness hover around 0.4 so the pedestal distribution has a property of a very small (close to 0) positive skewness.

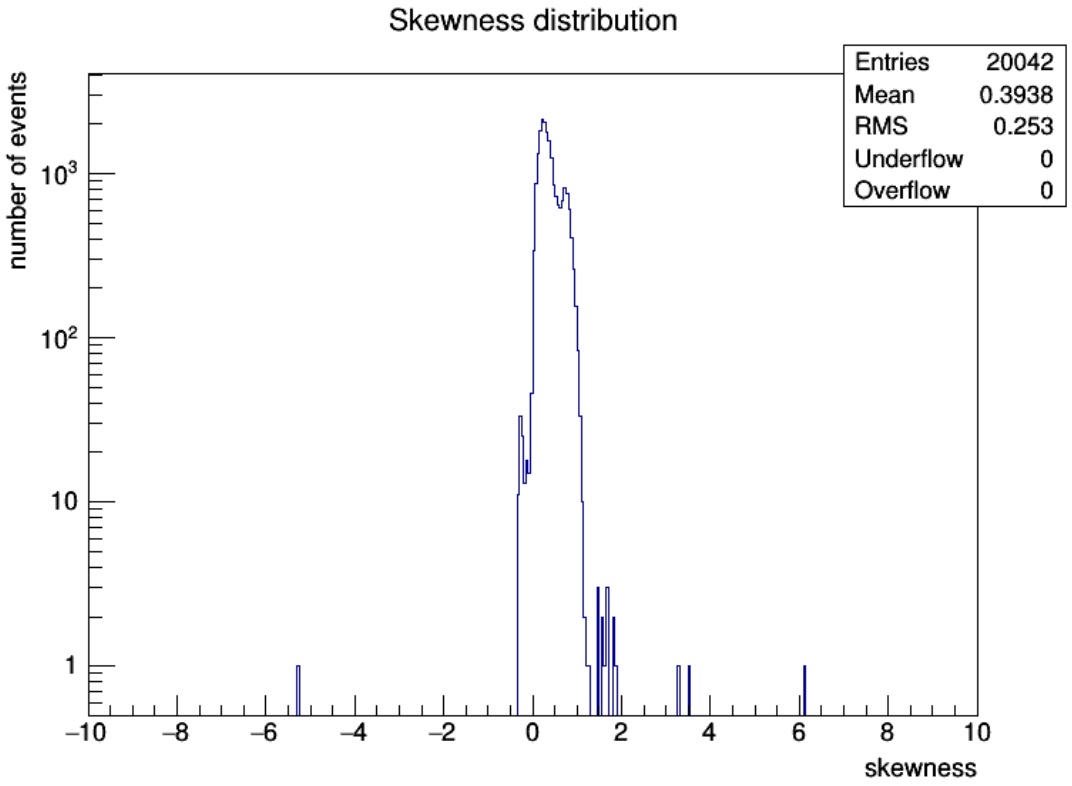

Figure 4-13: The distribution of the skewness

4.6. *Low and high ADC values readings*

The consecutive histograms were prepared to analyze the low and high-ADC value readings. To do so, the determination of the fractions of the low and high values of ADC counts as compared to the pedestal peak values was needed. The low-ADC values were defined when detected energy is lower than established threshold. The threshold T_{lij} for the low-ADC values of the i^{th} channel and j^{th} SVX chip was defined as:

$$T_{lij} = P_{ij} - 5 \cdot \sigma_{ij} \tag{4.3}$$

The subtraction of 5σ (so called 5 sigma cut) was chosen based on the silicon strip detectors characteristic found in [12]. This 5 sigma value was confirmed in this work and presented in section 6.2, where is shown that this condition rejects the majority of the noise without affecting the detector efficiency.

The high-ADC value is determined when the energy is greater than a given threshold T_{rij}. The definition of a T_{rij} is as follows:

$$T_{rij} = P_{ij} + 5 \cdot \sigma_{ij} \tag{4.4}$$

Figure 4-14 shows the distribution of the low-ADC value fraction where the fractions were calculated by dividing entries for the low-ADC values by entries to the pedestal peak. The pedestal peak P_p was determined using ADC values and is in the range as follows:

$$P_{ij} + 5\sigma_{ij} > P_p > P_{ij} - 5\sigma_{ij} \tag{4.5}$$

The pedestal peak contains most of entries what is shown in Figure 4-15. In Figure 4-16 is a distribution of the high-ADC value fraction. The fraction was calculated in a similar way to the low-ADC value fraction. The study showed that fractions of the low-ADC values have lower values than the high-ADC values fractions. It confirms that the pedestal distribution is slightly skewed towards the higher values what was also seen in section 4.5. The fractions are very low and this indicates that these are minor fluctuation of the pedestal value and they do not affect the determination of the mean and sigma. The following histograms (Figure 4-14, 4-15, 4-16) represent only channels, which had at least one entry for the low or high-ADC value.

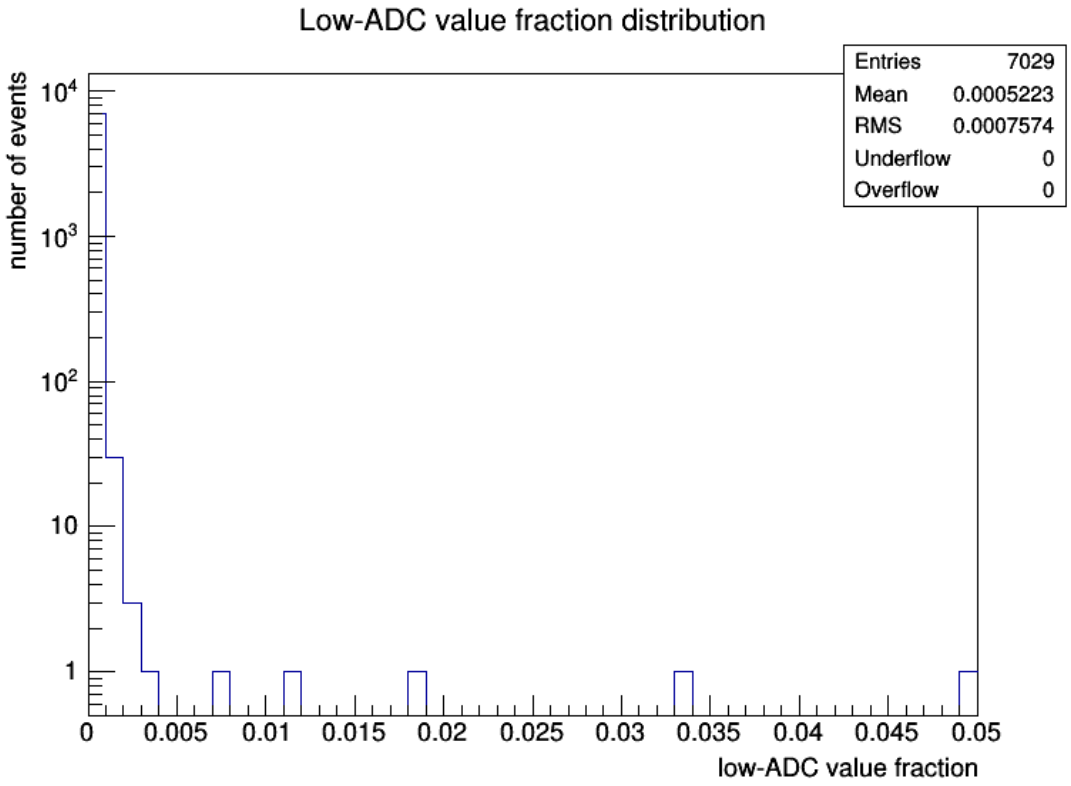

Figure 4-14: The distribution of the low-ADC value fraction

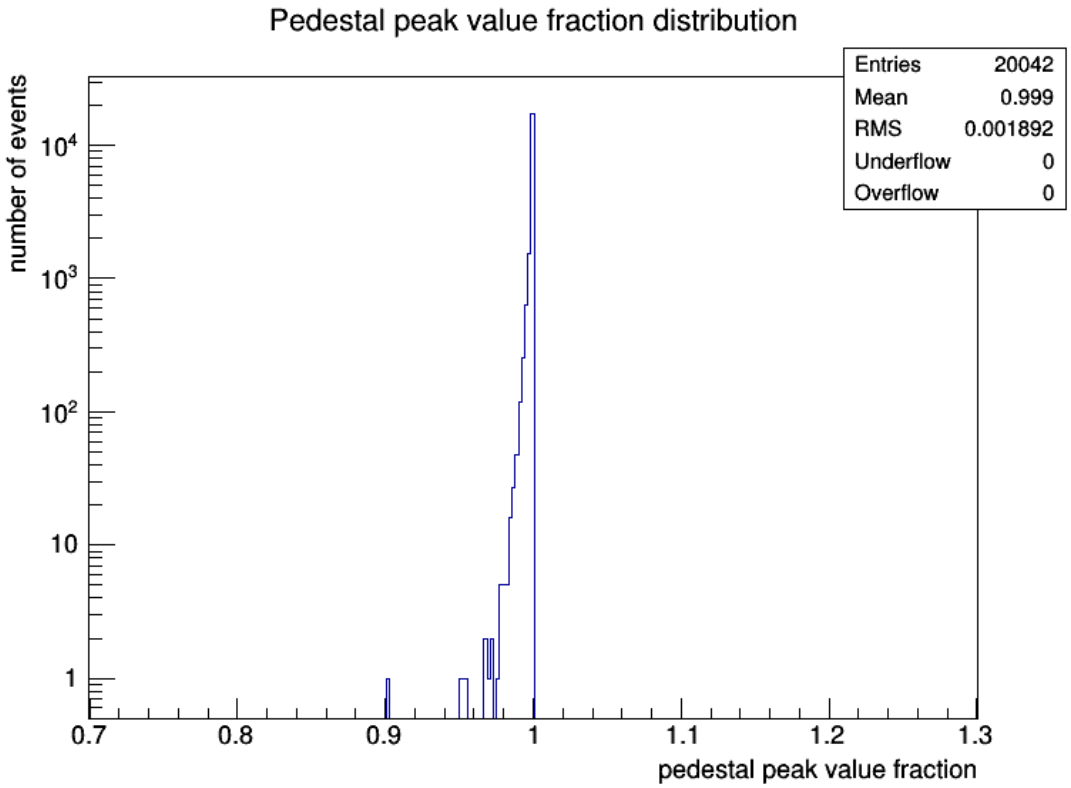

Figure 4-15: The distribution of the pedestal peak value fraction

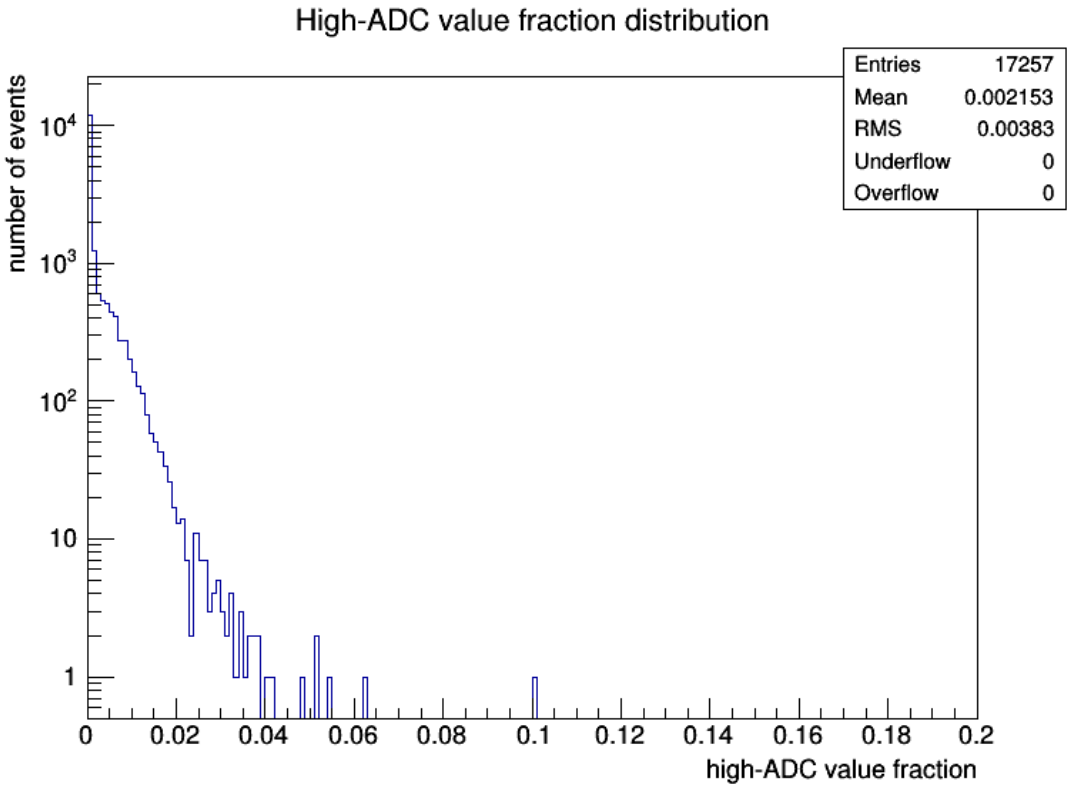

Figure 4-16: The distribution of the high-ADC value fraction

Figure 4-17 and Figure 4-18 present general outlines of the low-ADC value fractions and high-ADC value fractions for all channels for a given pedestal run. It is clearly seen that there are few channels with fraction of the order of a few percent. This test is also suitable to determine the range of the problem with noisy channels. Overall, the system works exceptionally well because the amount of channels with large low or high-ADC value fractions is insignificant compared to over 20 000 channels operating very well.

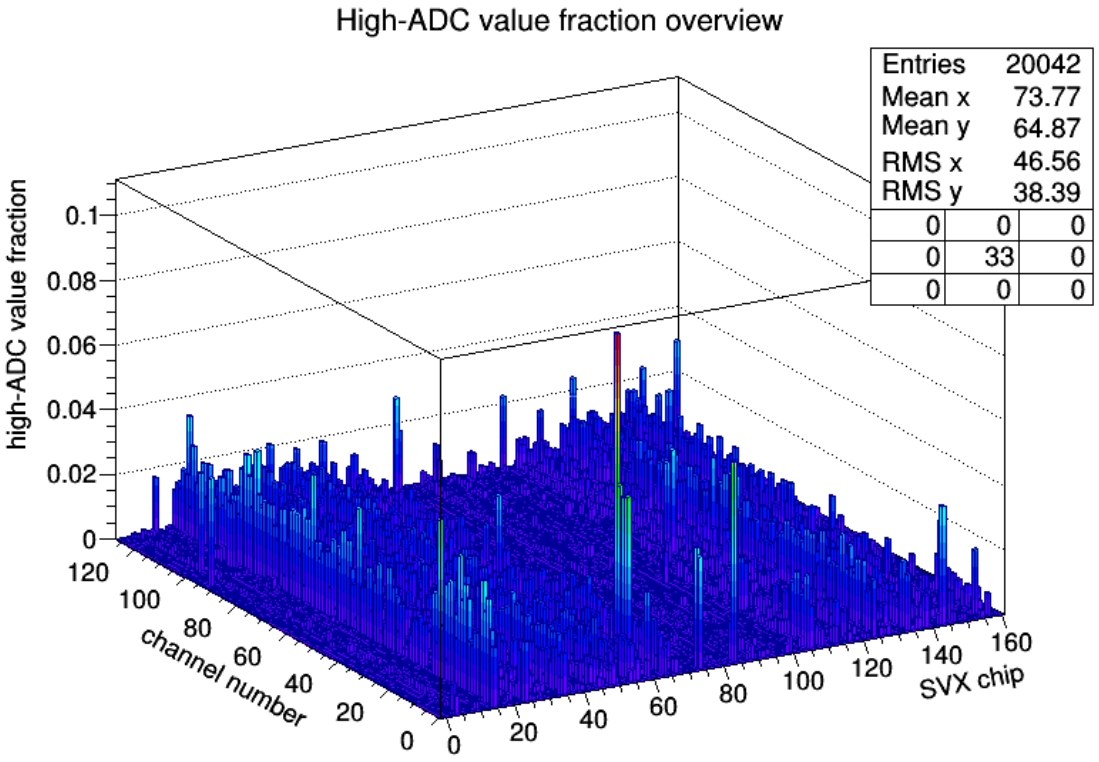

Figure 4-17: The distribution of the high-ADC value fraction for one pedestal run

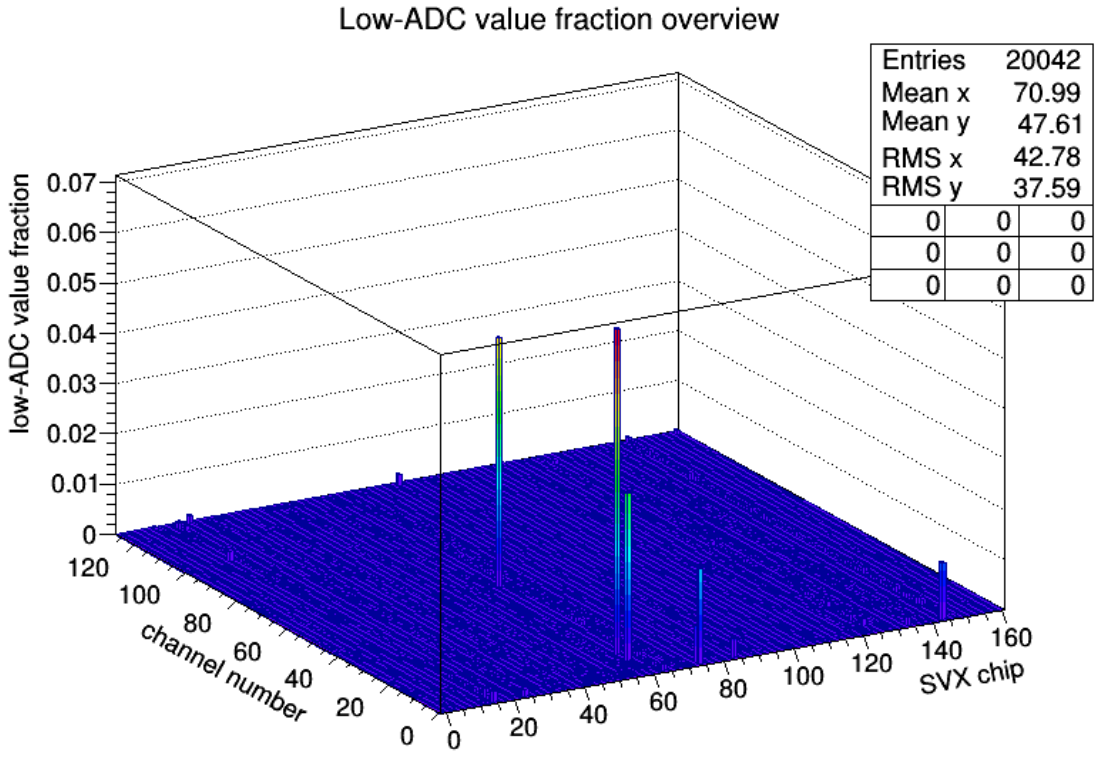

Figure 4-18: The distribution of the low-ADC value fraction for one pedestal run

4.7. *Pedestal subtraction*

After determining the value of the pedestal and concluding that for a given SVX readout chip the value of the pedestal is basically constant there is a question how to treat this pedestal. One of the ideas that was discussed was to subtract from the physics data the average pedestal P_{AVj} value of the given SVX chip retrieved from the STAR Data Base instead of the individual pedestal value for each channel determined offline in this work. The average value for a given SVX chip was calculated as follows:

$$P_{AVj} = \frac{1}{126}\sum_{i=2}^{127} P_i \tag{4.6}$$

where P_i is the true pedestal value of a given strip connected to the SVX chip. For plane E2DA average was determined for all 128 channels connected.

The sigma value was also averaged and defined as:

$$\sigma_{AVj} = \frac{1}{126}\sum_{i=2}^{127} \sigma_i \tag{4.7}$$

and σ_{AVj} is the average value of the sigma for a given SVX chip and σ_i is the sigma value for a given channel.

To validate if this assumption is correct I checked for every channel, how big is the difference between the pedestal value from the Gaussian fit for this channel and the average pedestal value P_{AVj} for a given SVX chip where those strip were connected. The study of all pedestal runs showed that this difference in most of events fluctuates around 0.4 ADC counts (the y-axis is in logarithmic scale); moreover, pedestal per channel is always greater than the average pedestal per SVX chip. This is partly due to the fact that the pedestal per channel is obtained from the Gaussian fit while the distribution of the pedestal has a small positive skewness (as it was pointed out in section 4.5). Thus, the value from the fit is greater than the average pedestal value for a given SVX chip retrieved from the STAR Data Base. Hence the average values in the STAR Data Base are histogram

mean values not values from fit. A sample distribution of differences is shown in Figure 4-19.

The difference between the sigma value from the fit and the average sigma from the STAR Data Base (Figure 4-20) is negative in most cases. The average sigma is greater than sigma per channel and the difference is approximately -0.2 ADC counts, which is very small. The logarithmic scale in these plots helped to show that for very few channels values significantly differs from the averaged values. This information helped with determining candidates for noisy channels.

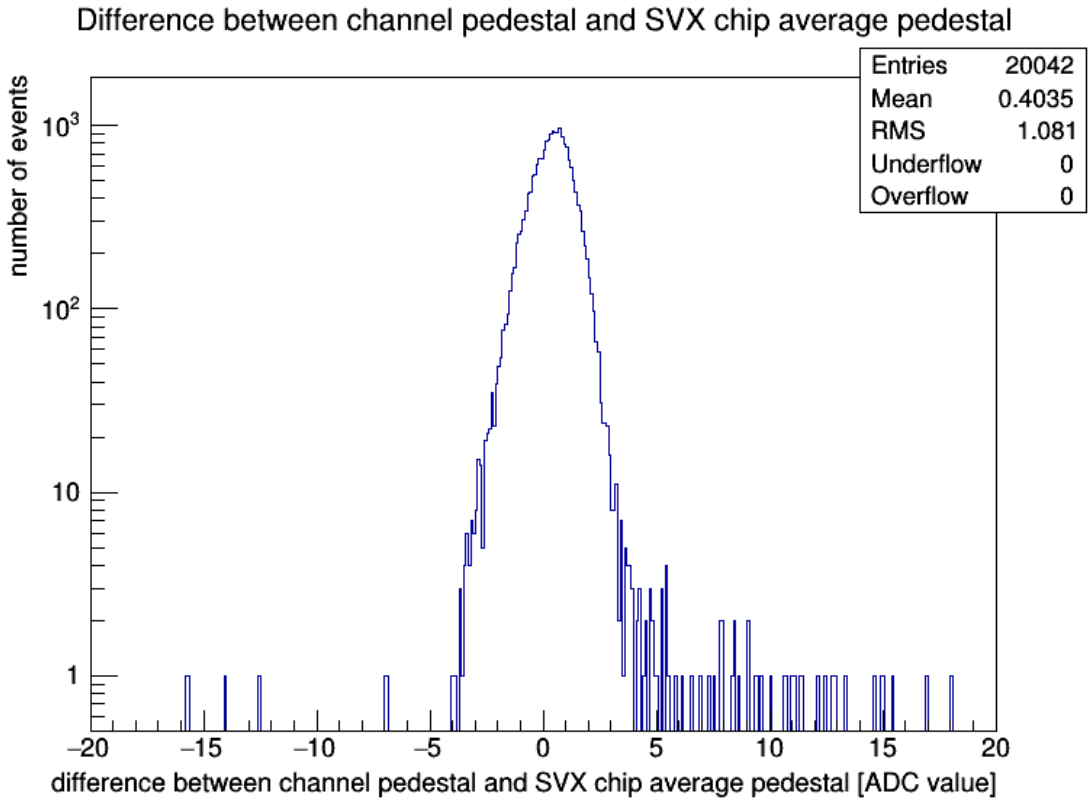

Figure 4-19: The difference between the channel pedestal and SVX chip average pedestal for one pedestal run

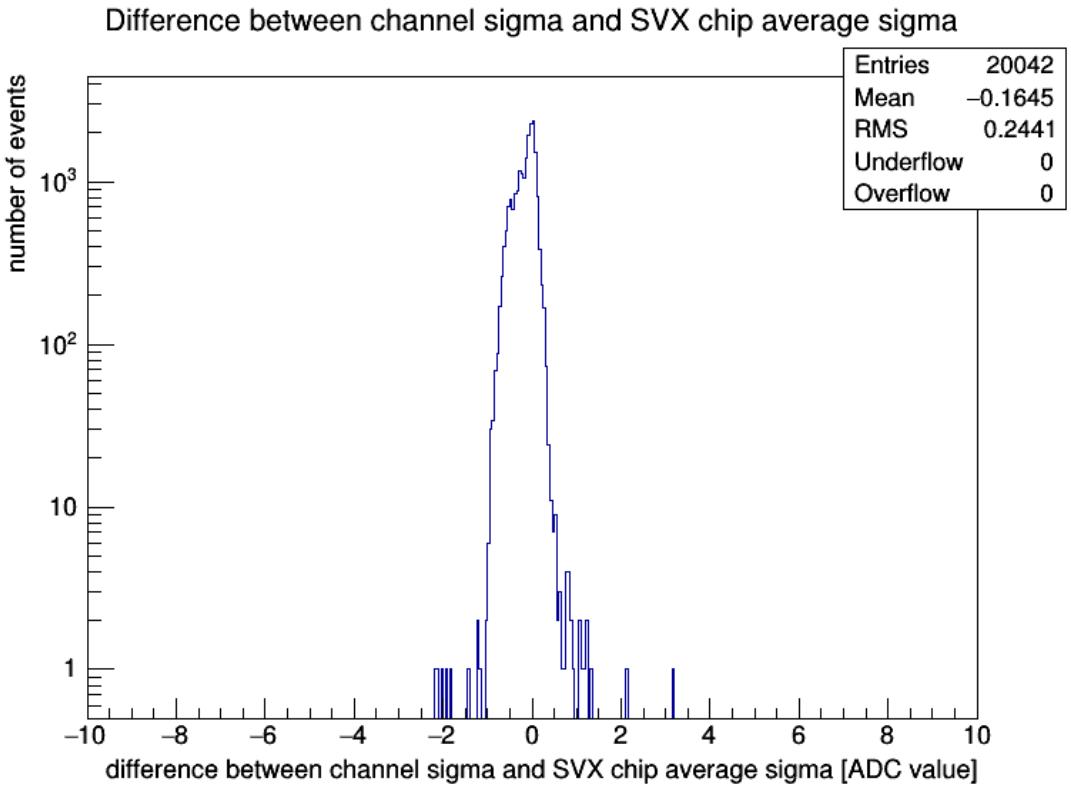

Figure 4-20: The difference between the channel value and SVX chip average sigma for one pedestal run

After this research one can conclude that using the average values of pedestal and sigma works well and it would give similar results as a channel-by-channel correction. Finally, the channel by channel pedestal was subtracted. That means that during physics runs each channel was corrected for a pedestal value obtained for that channel in corresponding pedestal run.

5. Noisy channels

5.1. Introduction

In this chapter noise of all 20 042 channels (strips) is examined to see if they function properly. With time they could be damaged so another necessary step in the characterization of the detector is to determine if there are defective channels, like so-called hot channels. The hot channel is a channel which gives unusually high ADC counts readings compared to others. Tests presented in Chapter 4 gave the general conclusion that irregularities present in detector planes do not affect much physics data and the number of noisy channels isn't a big concern. However, each additional hit may obscure data so in this chapter additional steps undertaken to determine the noisy channels are presented.

5.2. High sigma value

The two-dimensional histogram presented in Figure 5-1 shows that there are a few channels where the value of the sigma is greater than for other channels. Those a few channels have sigma about factor of two larger than the average sigma which is about 2 ADC counts. The important part of this study is to check how many channels tend to have the higher sigma value and whether it is a permanent feature (for most of the pedestal runs) or seldom (for some of the pedestal runs). Checking the variation of the sigma is an easy way to determine how many channels we suspect to be problematic. However, only the small fraction of the channels differs significantly from the mean value of sigma by a factor of two or more.

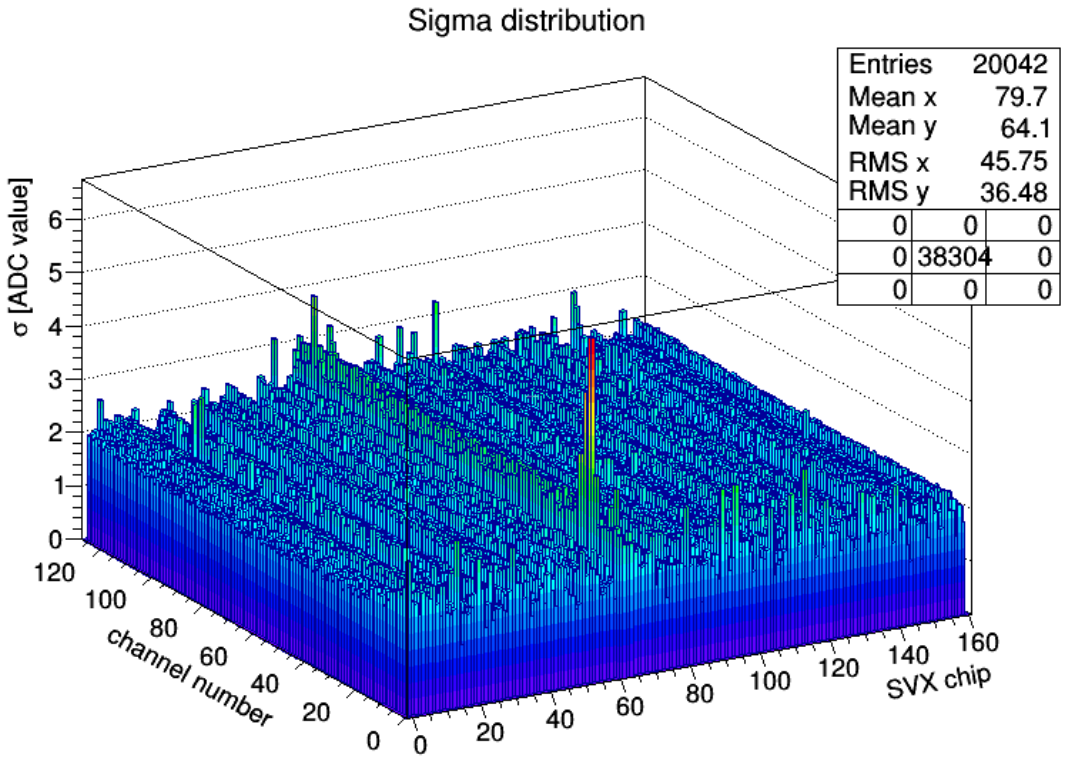

Figure 5-1: The distribution of sigma for a single pedestal run

5.3. *Non-Gaussian distribution*

As the section 4.4 has shown, properly working channel has a normal distribution (Figure 4-6) defined with the mean and sigma value. One way to check which channels are the suspected ones is to obtain the information whether their mean pedestal value from the Gaussian fit significantly differs from the average pedestal value for a given SVX chip retrieved from the STAR Data Base. In this case the channel started to be suspect when the absolute difference was equal or greater than 5 ADC counts. This value allows selecting a population of suspect channels. The majority of suspected channels are the first or the last channels of a given SVX chip. The example of this kind of problem is shown in Figure 5-2. The analysis of all pedestal runs shows that in each pedestal run approximately 51 channels are suspected to be hot channels what gives only about 0.3% out of 20 042 strips.

The similar study was performed to determine the candidates for noisy channels in case of large difference between sigma for a given channel and the average sigma for a given SVX chip retrieved from the STAR Data Base. The channel started to be suspected when the absolute difference was equal or greater than 1 ADC count, which is about three times standard deviation of the sigma distribution (Figure 4-11). The two-dimensional histogram presented in Figure 5-3 shows that only 21 channels exceed this threshold for a single pedestal run. Checking the suspect channels in the rest of pedestal runs confirmed that only negligible fraction of channels can be suspected to be hot channels.

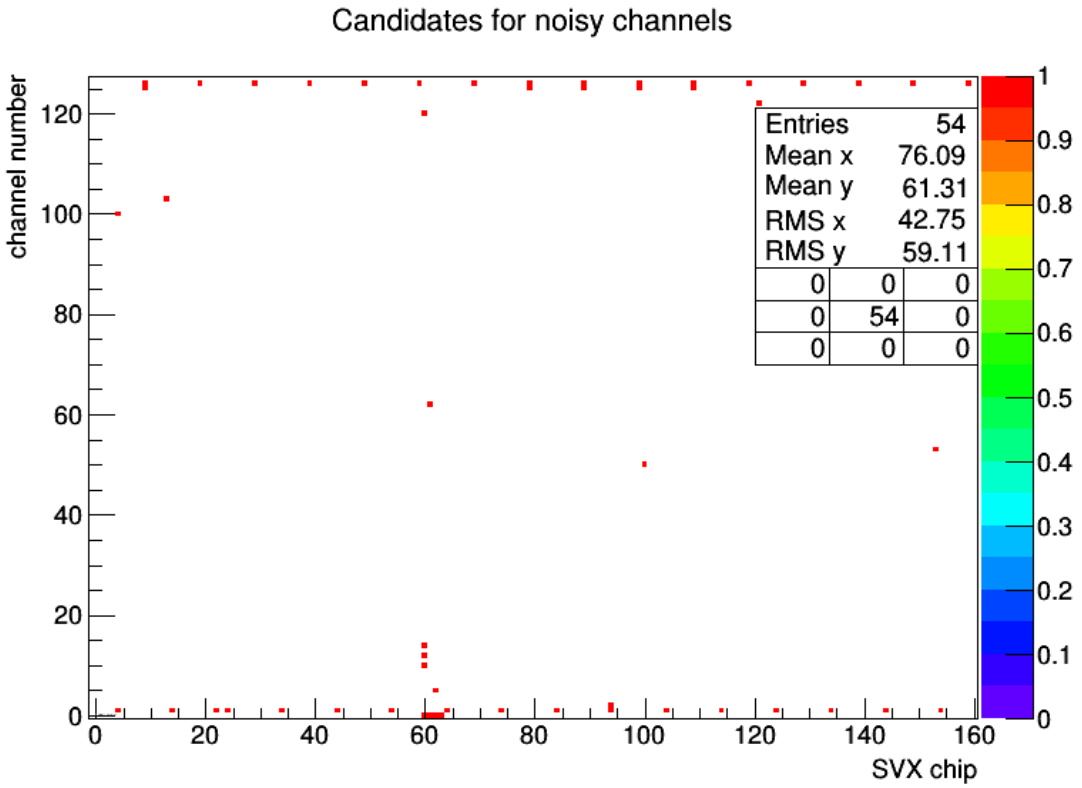

Figure 5-2: The suspected channels identified by the absolute difference between channel pedestal and SVX chip average pedestal being equal or greater than 5 ADC counts

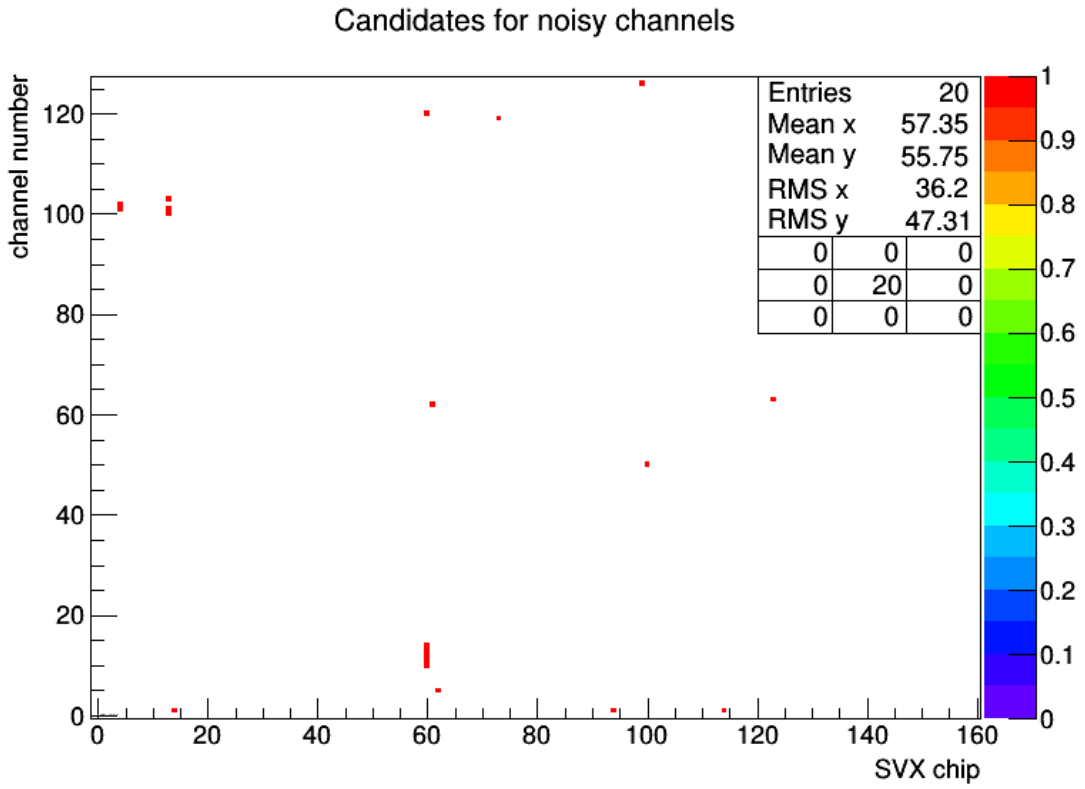

Figure 5-3: The suspected channels identified by the absolute difference between channel sigma and SVX chip average sigma being equal or greater than 1 ADC count

5.4. High-ADC values readings

Another way to check for improperly working channels was to select those channels which had considerable greater high-ADC value fractions than the average. A channel is defined as a hot channel if there were multiple readings with energy greater than 20 ADC counts above the pedestal. Figure 5-4 presents the outcome of this analysis. Only a few channels look like they could be candidates for the hot channels but especially two of them seem to have a problem. Further analysis confirmed that there are only two potentially hot channels: a channel number 11 and a channel number 13 of SVX chip number 060. Eventually they were not excluded from analysis because the probability that hits of interests are located in affected strips is very low and equals to 0.8% for each channel.

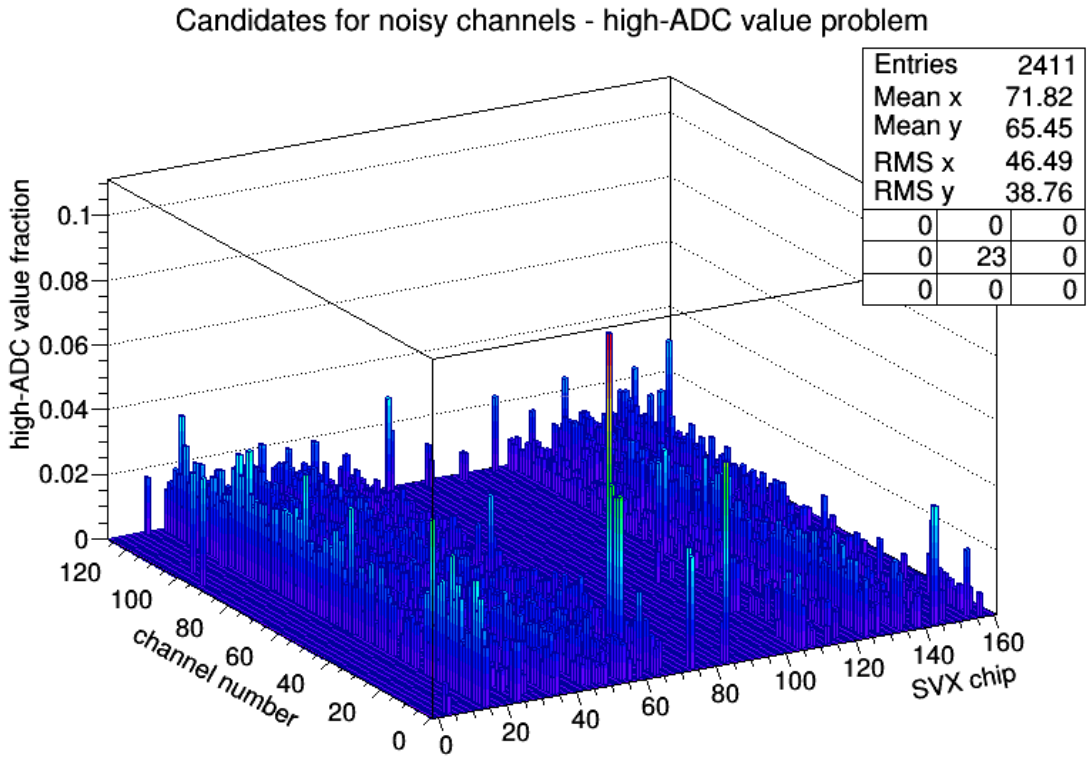

Figure 5-4: The histogram presents fractions of entries for the high-ADC values

6. Clusters and hit reconstruction

6.1. Clusters

The pedestal subtraction and defining noisy channels are not the only steps taken in order to obtain real hit from a particle, called here also a physics hit. The next step is to determine the optimal threshold that excludes the noise hits. The noise status can be diagnosed not only with the study of pedestal run but also with the analysis of physics run.

A real physics hit (hit of interests) is defined as hit which comes from the elastically scattered proton detected by the SSDs. Information about particle and the track of the particle is stored in a cluster. The cluster is a set of consecutive strips which detected particle with energy greater than a threshold which is used to eliminate noise. Each cluster contains three parameters to describe detected particle [12]:

- energy loss (dE/dx) of the particle,
- position of the cluster,
- size, it is a number of the consecutive strips with an ADC value greater that the certain threshold.

These three parameters give complete information about the particle.

6.2. n-sigma cut

Figure 6-1 shows clusters energy (energy loss of the particle) distribution. It is easy to observe a peak on the left side of the main peak, the latter being energy deposited by a particle. The first, the low energy peak, represents the statistical noise of a given Roman Pot. As mentioned in section 4.1, statistical noise is represented as a standard deviation of a pedestal value. It is clearly seen in Figure 6-1 that the signal is well separated from the noise. To eliminate the random (statistical) noise from the data sample additional cut has to be applied during clustering. This cut is called the n-sigma cut and it is represented by the threshold S_c defined as:

$$S_c = n \cdot \sigma_j \tag{6.1}$$

where n is a constant selected to get rid of as much random noise as possible as well as to obtain high detection efficiency. The σ_j is statistical noise for a given SVX chip. To find an optimal value, number of possible values has been checked. Further analysis showed that 5 σj cut (Figure 6-2) is an optimal one where the vast majority of noise has been eliminated, residual part of noise is well separated and there is a large signal to noise ratio.

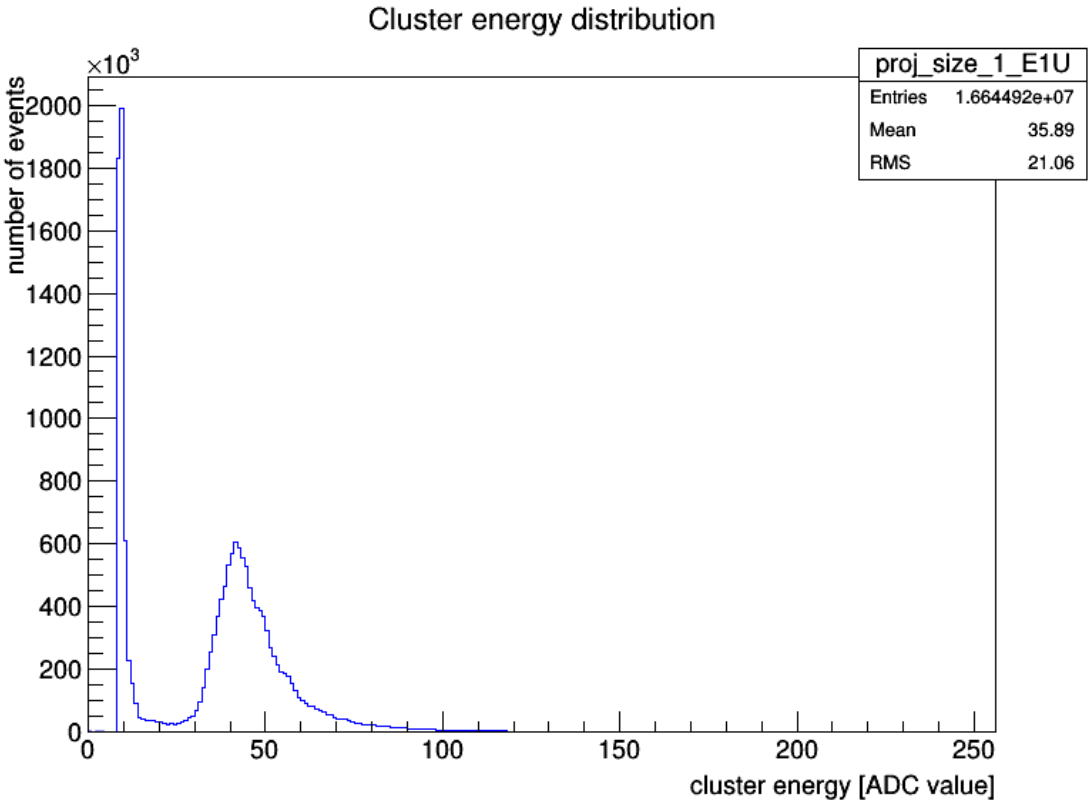

Figure 6-1: The cluster energy distribution for Roman Pot E1U after 4 sigma cut

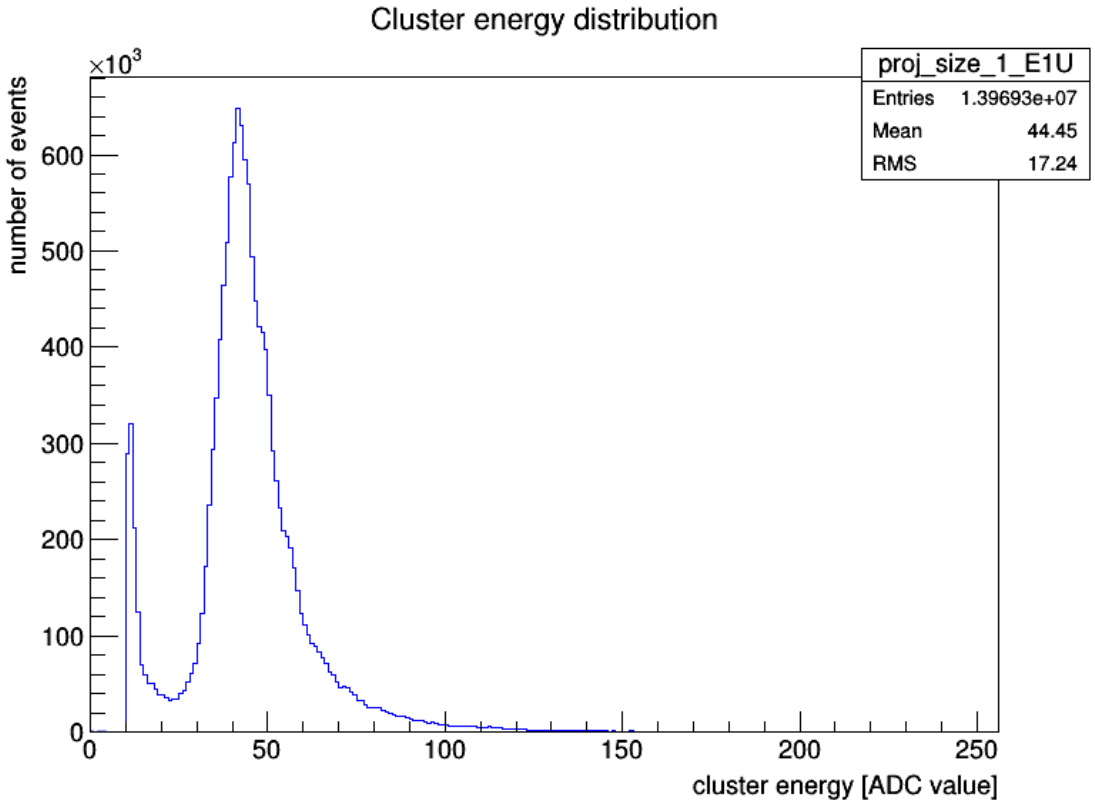

Figure 6-2: The cluster energy distribution for Roman Pot E1U after 5 sigma cut

To eliminate the remaining part of noise another condition was applied. Defining this condition involves using the knowledge that dE/dx for high energy protons which are detected by Roman Pots, follows the Landau distribution presented in Figure 6-3. It was found that the threshold of 20 ADC counts as a minimal loss of the particle energy allows removing practically all of noise without losing events of interest. A histogram with two conditions applied is shown in Figure 6-4.

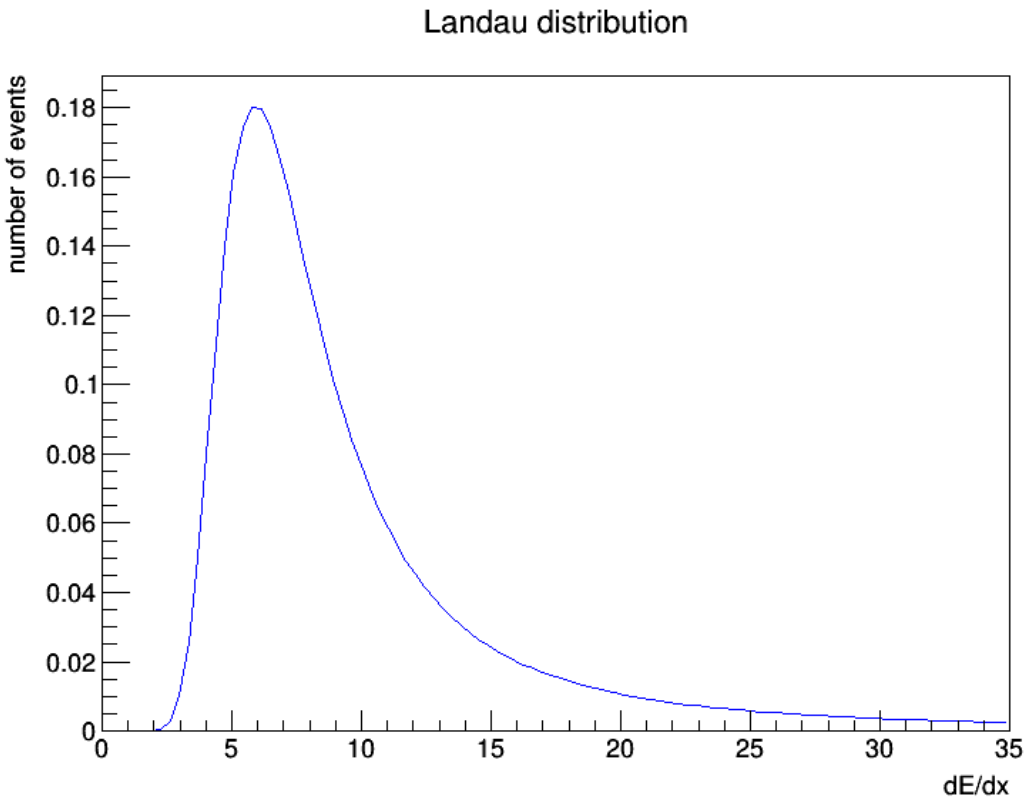

Figure 6-3: The Landau distribution

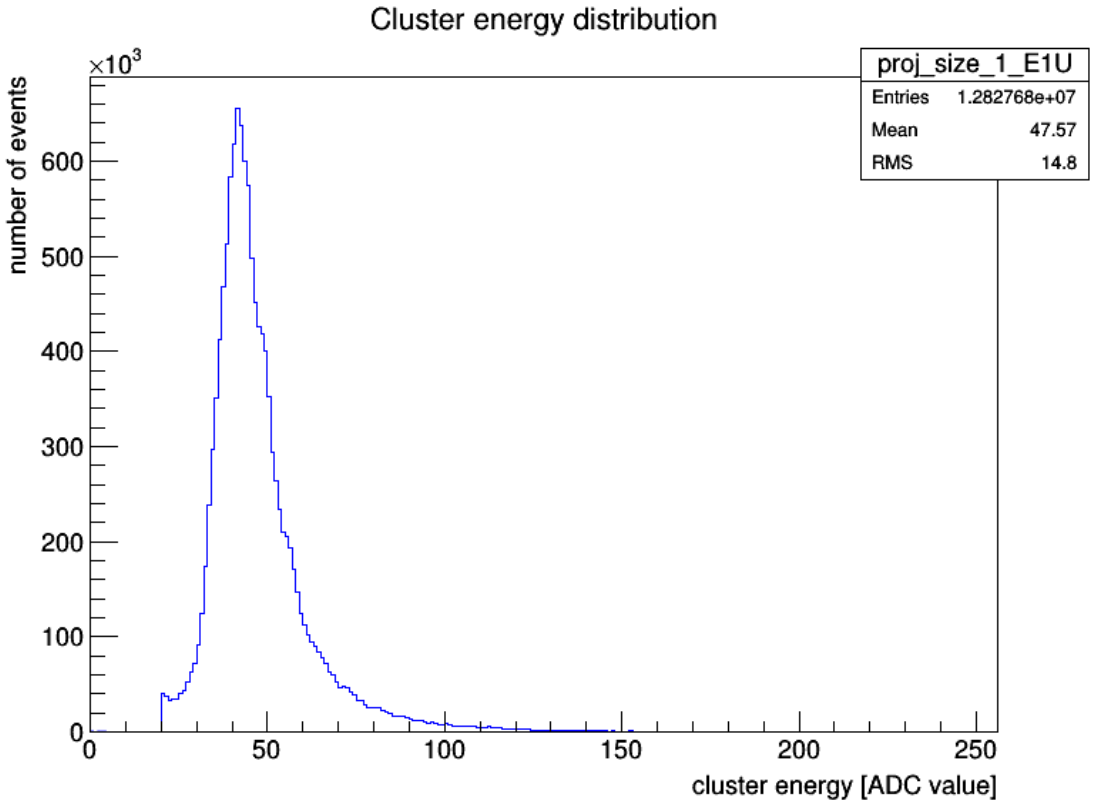

Figure 6-4: The cluster energy distribution for Roman Pot E1U after 5 sigma cut and cut of 20 ADC counts

6.3. The elimination of the background

Further steps need to be taken because physics data are still affected by background. Noise elimination hasn't solved the whole problem since the background consists of the hits that come from particles that are not protons. This requires using the following steps to obtain as clean data sample as possible. The solution to this issue is to limit cluster size (i.e. the number of consecutive strips in a cluster). Since the trajectory of scattered protons (particles of interest) is almost perpendicular to the detector, one expects the maximum size of the cluster as a few strips. The histogram of energy vs cluster size (Figure 6-5) shows that the vast majority of clusters have a size of 1 or 2 strips. Based on Figure 6-6 we decided to accept those clusters that have size not greater than 4 strips.

Applying condition on the cluster size still does not give the certainty that all background has been subtracted. Another necessary step is to limit the number of clusters per event. For the elastically scattered protons, there is only one particle passing through the detector planes. It implies that there should be only one cluster per event in the detector plane. This assumption is confirmed in Figure 6-7 which shows the distribution of the number of clusters per one sample plane. In great majority of events there is only one cluster per plane. However, some events have more than 40 clusters, consequently, limit on the number of cluster per event is essential to get samples suitable for analysis.

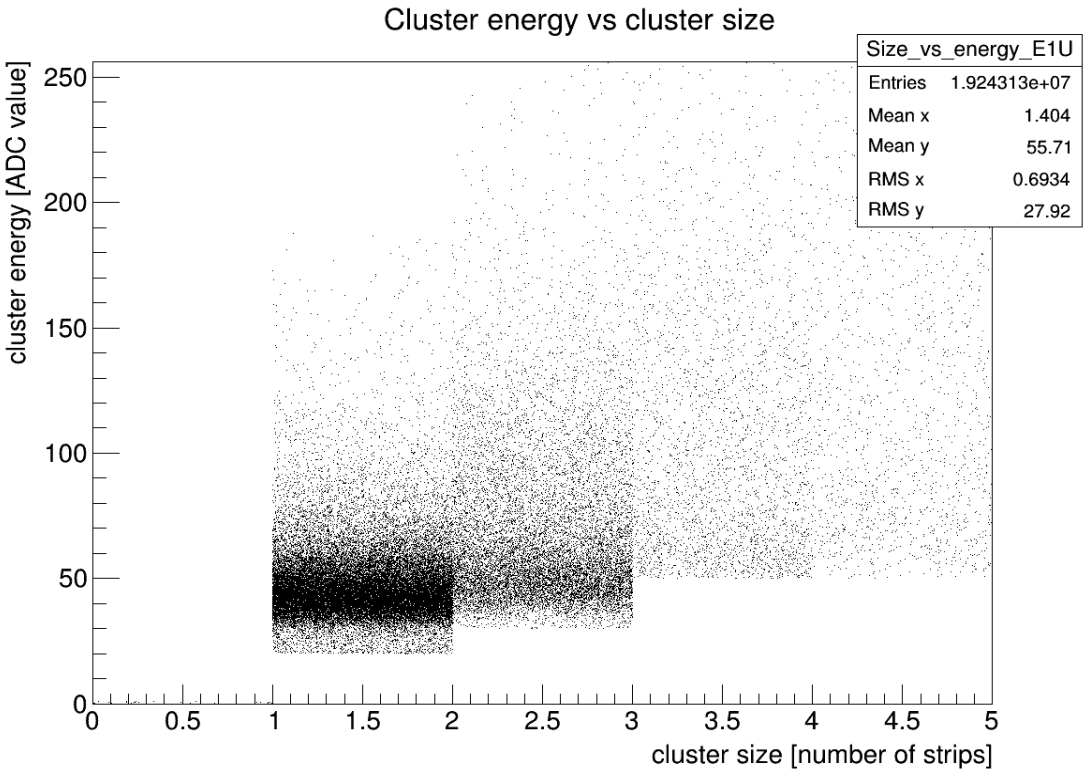

Figure 6-5: The cluster energy vs cluster size for Roman Pot E1U

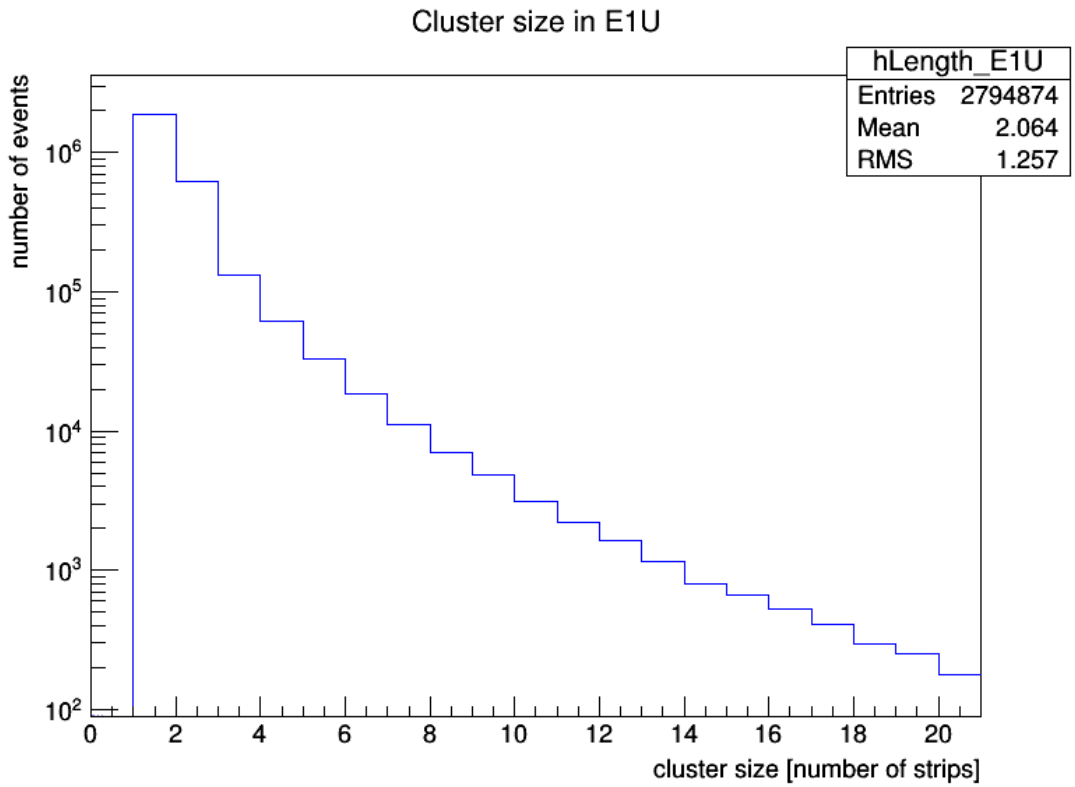

Figure 6-6: The cluster size distribution after 5 sigma cut and cut of 20 ADC counts

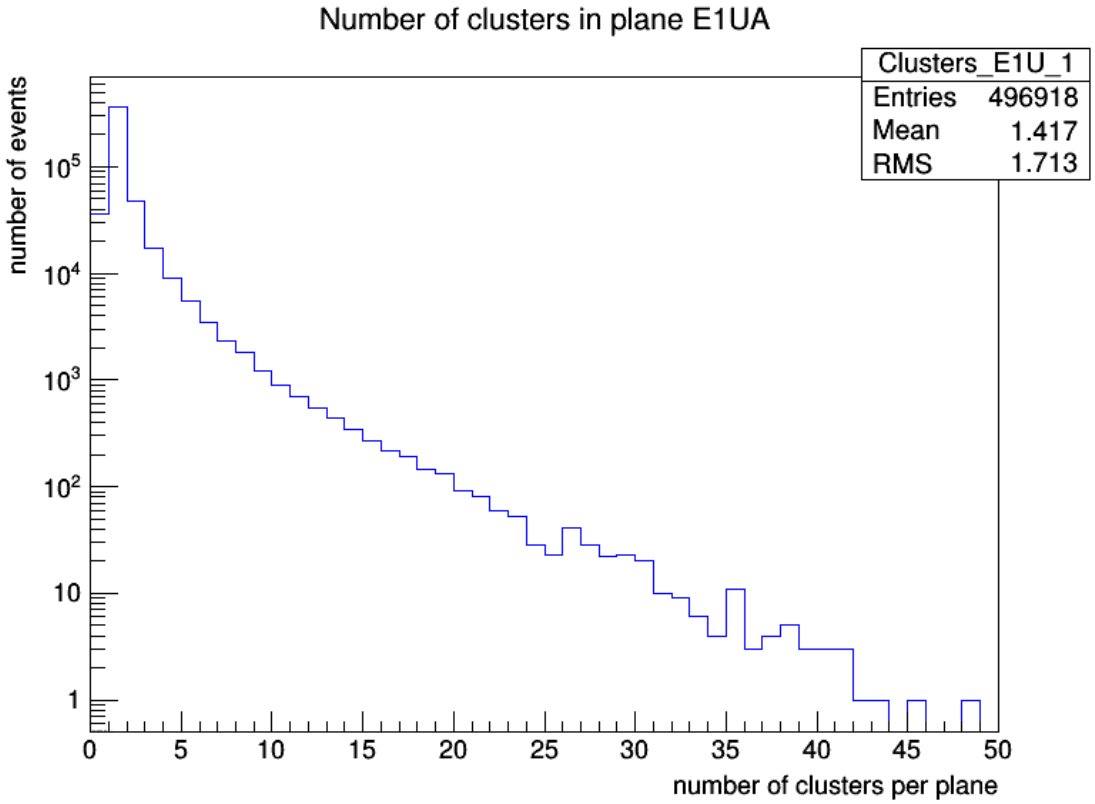

Figure 6-7: The number of clusters per plane distribution for Roman Pot E1U after 5 sigma cut and cut of 20 ADC counts. The logarithmic scale is on y-axis.

6.4. Matching clusters

The next step in background reduction is to check the position difference between corresponding clusters in two planes measuring the same coordinate in one Roman Pot. If the particle of interest passed through the Roman Pot, the cluster position in one plane should be similar to the position of matched cluster in the corresponding plane in the same Roman Pot. An example distribution of the position difference in planes with the vertical strips in Roman Pot E1U shows that in most of the cases there is no difference in the cluster positions in corresponding planes (Figure 6-8, Figure 6-9). The distribution in Figure 6-11 shows that the difference in planes measuring Y coordinate is approximately equal to 100 µm which indicates that there is one strip difference in cluster position in the corresponding planes (Figure 6-10). One needs to consider those ranges to obtain data samples without noise. Based on those plots we found that to accept hit as a hit of interest absolute difference must be of the order of 100 µm. Applying this

condition, accepting events which have cluster size not greater than 4 strips and the use of cuts presented in section 6.2 allowed obtaining energy distribution for golden event shown in Figure 6-12. A golden event is an event of interest (detected proton by two corresponding Roman Pots) without noise and hits of other particles.

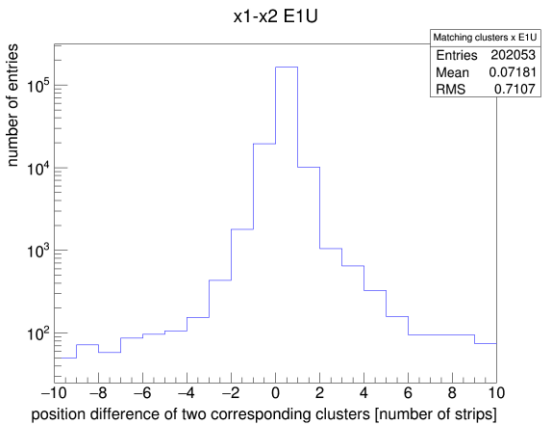

Figure 6-8: The difference of clusters positions in planes measuring x coordinate E1U [number of strips]

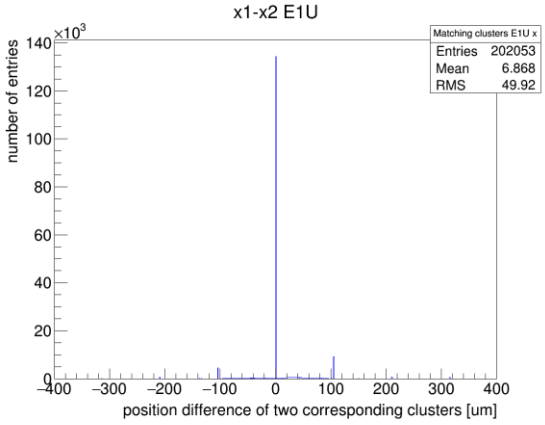

Figure 6-9: The difference of clusters positions in planes measuring x coordinate E1U [μm]

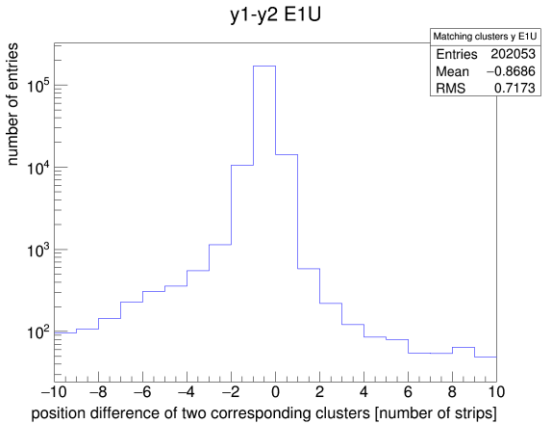

Figure 6-10: The difference of clusters positions in planes measuring y coordinate E1U [number of strips]

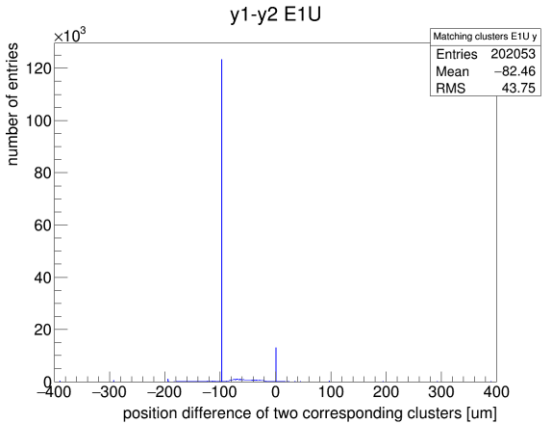

Figure 6-11: The difference of clusters positions in planes measuring y coordinate E1U [μm]

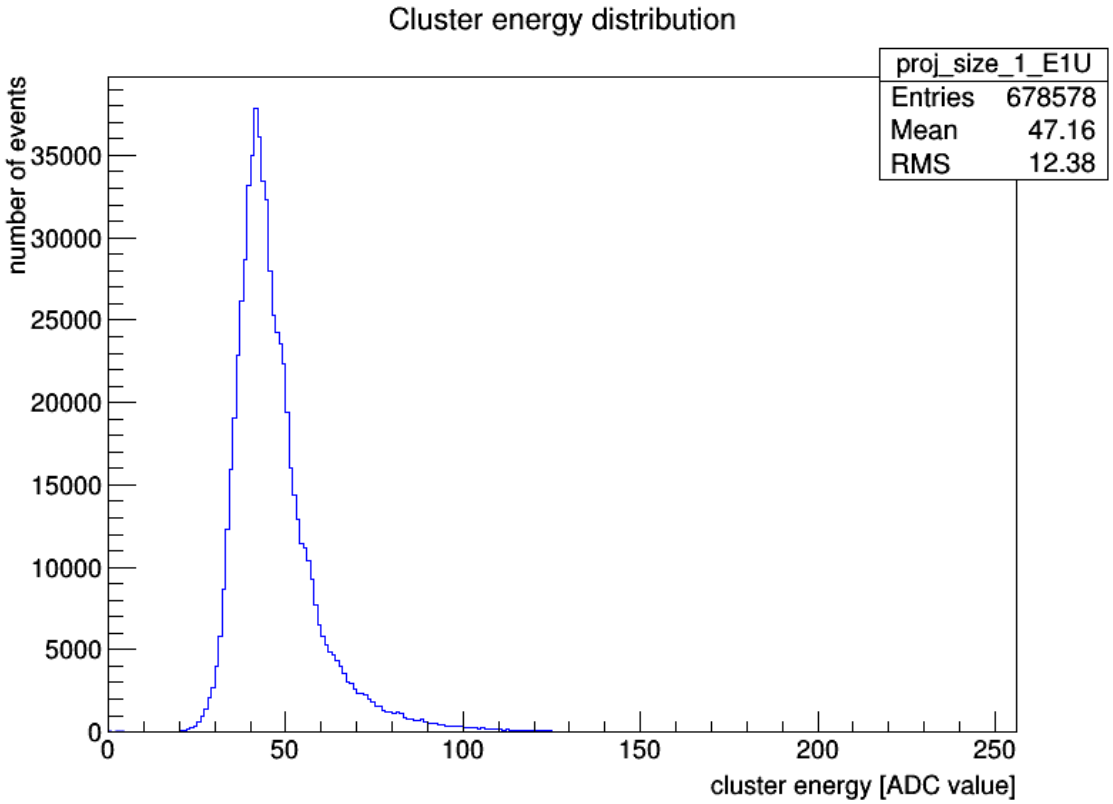

Figure 6-12: The distribution of the cluster energy after all cuts for E1U

In this thesis, the essential characteristics of the silicon micro-strip detectors used in the STAR experiment were determined. There are also other properties of the SSDs that could be studied, for example, a signal to noise ratio and their efficiency (more details about such procedures can be found in [12]). The signal to noise ratio can be determined by comparing the peak of the Landau distribution, which is about 40 ADC counts to the average sigma of pedestal noise, which is about 2 ADC counts. Thus giving a signal to noise ratio of at least 20.

7. Summary

The primary goal of this thesis was to characterize the silicon micro-strip detectors used by the STAR experiment to detect forward protons. The study showed that pedestal and noise fluctuate around 80 ADC counts and 2 ADC counts, respectively and the levels of pedestal and noise are stable over time. The investigation of all strips showed that there are only two potentially hot channels out of about 20 000 (the channel number 11 and 13 of the SVX chip number 060). The analysis of cluster energies allowed to determine two necessary thresholds: 5 sigma cut and cut of 20 ADC counts, resulting in the removal of practically all noise without losing events of interest. The maximum size of the cluster was established as 4 strips and the absolute difference between corresponding clusters positions as 100 μm.

Given all the above the performance of the SSD is determined to be very good. The observed variations are minimal and the high signal to noise ratio of 20 or more should allow efficient physics analysis.

Bibliography

[1] RHIC accelerator website, https://www.bnl.gov/rhic/

(accessed February 2, 2016).

[2] Guryn W., private communication

[3] Sikora R., *Study of elastic proton-proton scattering with the STAR detector at RHIC*. Master Thesis, AGH University of Science and Technology, Cracow 2014

[4] The physics of the RHIC, https://www.bnl.gov/rhic/physics.asp

(accessed February 2, 2016).

[5] Spin Physics, https://www.bnl.gov/rhic/spin.asp

(accessed February 10, 2016).

[6] STAR experiment website, https://www.star.bnl.gov/

(accessed February 2, 2016).

[7] PHENIX experiment website, http://www.phenix.bnl.gov/

(accessed February 2, 2016).

[8] Koralt I., *Measurement of polarized proton-proton elastic scattering at Relativistic Heavy Ion Collider (RHIC),* Doctor of Philosophy Thesis, Old Dominion University, 2013

[9] The STAR Detector, https://www.bnl.gov/rhic/STAR.asp

(accessed January 10, 2016).

[10] Guryn W., Physics with tagged forward protons at RHIC, *Acta Phys.Polon.*

B40 (2009) 1897-1908

[11] Bültmann S., Chen W., Chiang I.H, Chrien R.E., Drees A., Gill R.L. et al, *The PP2PP experiment at RHIC: silicon detectors installed in Roman Pots for forward proton detection close to the beam,* Nucl.Instrum.Meth. A535 (2004) 415-420

[12] Obrębski T., *Study of the characteristics of the silicon detectors used to measure protons in STAR experiment at RHIC*, Engineering Thesis, Faculty of Physics, Warsaw University of Technology, 2010.

[13] Kociubiński A.,*Krzemowe detektory paskowe,* http://www.if.pw.edu.pl/~pluta/pl/dyd/mfj/zal03/kociubinski/wstep.html (accessed January 22, 2016).

[14] Guryn W., Central Production with tagged forward protons and the STAR detector at RHIC*, Frascati Physics Series*, Vol. XLVI (2007)

[15] Glueball– Wikipedia, the free encyclopedia, https://en.wikipedia.org/wiki/Glueball (accessed February 5, 2016).

[16] Sikora R., *Naming convention and layout of the Roman Pot Phase II* subsystem in the STAR experiment, STAR Technical note* (unpublished), 2014

[17] ROOT software website, https://root.cern.ch/

(accessed December 17, 2015).

[18] Rouse M., *Skewness,* http://whatis.techtarget.com/definition/skewness (accessed January 3, 2016).